Chapter 2

The Application of Fragment-based Approaches to the Discovery of Drugs for Neglected Tropical Diseases

Christina Spry[1,*] and *Anthony G. Coyne*[2]

Introduction

The term *neglected tropical disease* (NTD) is used to describe a diverse collection of communicable diseases prevalent in tropical and subtropical regions, which predominantly affect the poor. The World Health Organization (WHO) currently identifies a set of twenty diseases,[†] chiefly caused by parasites, bacteria and viruses, as priority NTDs (WHO 2018a). Although these diseases have not attained the notoriety of the "big three" infectious diseases—malaria, tuberculosis and HIV—most are highly debilitating, several cause chronic diseases, and some are lethal. They currently affect more than a billion people in 149 countries (WHO 2018a) and impart a substantial economic and social burden, thereby perpetuating the cycle of poverty and disease. Through implementation of five main strategies (preventative chemotherapy, innovative and intensified disease management, vector ecology and management, veterinary public health services and the provision of safe water, sanitation and hygiene), great strides have been made toward the goals of controlling, eliminating and eradicating NTDs set forth by the WHO in 2012 (WHO 2017). However, in order to meet targets set for 2020 and beyond, it has become evident that new control tools, including drugs, are needed. For some NTDs no safe, affordable and orally active drugs are available, and where they are, alternatives are required for combination therapies and as backups for when efficacy is lost and/or resistance emerges. Despite the high NTD burden, in the period between 2000 and 2011, just 0.6% of new therapeutics were for neglected diseases and none of these were new chemical entities (Pedrique et al. 2013), highlighting the unmet medical need.

[1] Research School of Biology, The Australian National University, ACT, 2601, Australia.
[2] Department of Chemistry, University of Cambridge, Cambridge, CB2 1EW, United Kingdom.
* Corresponding author: christina.spry@anu.edu.au

[†] At of the time of publication, the WHO NTD portfolio includes: (1) Buruli ulcer, (2) Chagas disease, (3) Dengue and Chikungunya, (4) Dracunculiasis, (5) Echinococcosis, (6) Foodborne trematodiases, (7) Human African trypanosomiasis, (8) Leishmaniasis, (9) Leprosy, (10) Lymphatic filariasis, (11) Mycetoma, chromoblastomycosis and other deep mycoses, (12) Onchocerciasis, (13) Rabies, (14) Scabies and other ectoparasites, (15) Schistosomiasis, (16) Soil-transmitted helminthiases, (17) Snakebite envenoming, (18) Taeniasis, (19) Trachoma, and (20) Yaws.

Phenotypic (or whole-cell) screening has dominated over target-based approaches in drug discovery for NTDs (Gilbert 2013, Martin-Plaza and Chatelain 2015, Behnam et al. 2016). There are two main reasons:

(i) The success of any target-based approach is underpinned by the careful choice of a well-validated drug target. In the case of NTDs, few validated drug targets have been identified. This, at least in part, is because the genetic tools for target validation in the pathogens causing NTDs (except perhaps *Trypanosoma brucei*) are lacking, and the modes of action of existing drugs are poorly understood (Gilbert 2013).

(ii) In phenotypic screens, molecules with access to a given molecular target, which possess activity in the context of the cell (where permeability barriers and efflux mechanisms exist and mechanisms of metabolic plasticity and regulation operate), are identified from the onset. This is particularly advantageous for pathogens with intracellular stages such as *Leishmania* (the cause of leishmaniasis).

Despite the above advantages of phenotypic screening for hit identification, subsequent hit-to-lead and lead optimization can be a significant challenge. Elucidation of the molecular target(s) of a hit greatly facilitates hit-to-lead optimization, however, this is no trivial task. Metabolomic analysis is one approach that has been used successfully to provide clues to the mode of action of antitrypanosomal and antileishmanial compounds (Vincent and Barrett 2015). Nonetheless, even when the molecular target of a phenotypic screening hit can be confidently identified, improving target affinity while also achieving the required drug-like properties is challenging and requires intensive medicinal chemistry efforts.

Over the past two decades, fragment-based approaches have gained traction as alternative and complementary hit finding mechanisms to target-based and phenotypic high-throughput screening (HTS) (Erlanson et al. 2016). By contrast with HTS, which involves screening of a large library (typically tens to hundreds of thousands) of drug-like compounds in a high-throughput assay, a classical fragment-based approach begins with the screening of a small library (typically 1000–5000) of fragments (chemicals of low molecular weight and complexity), primarily using biophysical techniques. The goal of a fragment screen is to identify chemicals that bind a target efficiently. As a consequence of their low molecular weight and size, fragments invariably bind with low affinity, and therefore metrics are used that attempt to normalize affinity for properties such as molecular weight. The most popular metric is ligand efficiency (LE), in which the free energy of binding of a compound is divided by the number of non-hydrogen atoms (NHA) that compound has (reported in units of $kcal.mol^{-1}.NHA^{-1}$) (Hopkins et al. 2004). Provided sufficient structural information is available, weakly, but efficiently binding fragment hits can be elaborated iteratively into higher affinity binders with drug-like properties. Fragments are commonly elaborated by *growing* (the iterative addition of moieties designed to pick up interactions in neighboring regions of a binding site), *merging* (the amalgamation of fragments binding in overlapping binding sites into a single molecule), or *linking* (the fusion of two fragments binding in adjacent regions of a binding site through a chemical linker). For a review of fragment screening approaches and discussion of fragment elaboration strategies, the reader is referred to Scott et al. (2012).

Although typically only compatible with target-based approaches, fragment-based approaches have a number of advantages over HTS approaches, the first of which is that fragments form high quality interactions with a target. This stems from their low complexity and, as a consequence, the greater probability they will complement a binding pocket as compared with more complex drug-like molecules where the optimal binding modes of key moieties may be hindered by unfavorable interactions with other moieties (Ham et al. 2001). The second reason is that fragments are efficient probes of chemical space; the chemical space associated with molecules of drug-like size is estimated to be 13 orders of magnitude greater than that associated with fragment-sized chemicals (Ruddigkeit et al. 2012, Erlanson et al. 2016). Hence a small fragment library more efficiently samples the fragment chemical space than a large library of drug-like compounds samples drug-like chemical space. For this reason, fragment-based approaches offer a means by which to overcome the chemical diversity limitations of HTS libraries. Higher hit rates are encountered in fragment-based approaches, providing more choice for chemical starting points, and smaller and more easily maintained libraries are used, facilitating implementation of fragment-based approaches also in an academic setting. Fragment-based approaches are now used widely in academia

and industry and have produced more than 45 clinical candidates and at least four drugs approved by the US Food and Drug Administration (Erlanson et al. 2016, Peplow 2017, Erlanson 2019).

In this chapter, we describe how fragment-based approaches are being applied in projects aimed at the discovery of new drugs for NTDs, either alone or in conjunction with HTS. The examples discussed, which have been classified according to pathogen, highlight the power of fragment-based approaches to reveal binding hot-spots and novel allosteric binding sites, and to identify efficient starting points for drug discovery. They also show how fragment-based approaches can facilitate optimization of hits identified by other means and enable careful control of drug-like properties during the optimization of a chemical series.

Fragment-based Approaches in Antitrypanosomal Drug Discovery

Chagas disease and Sleeping Sickness are two NTDs caused by protozoan parasites of the genus *Trypanosoma*. Chagas disease, which is also known as American trypanosomiasis, affects approximately 6–7 million people, predominantly in Latin America (although increasing numbers of cases are being detected elsewhere around the world (Schmunis and Yadon 2010)), and results in over 10,000 deaths annually (WHO 2017, 2018b). The disease is caused by *Trypanosoma cruzi*, which is primarily transmitted by the triatomine bug, but can also be transmitted through blood transfusion from infected donors, or from mother to child during pregnancy or childbirth. There is no vaccine for Chagas disease, but the disease can be cured with the antiparasitic drugs benznidazole or nifurtimox if treatment is initiated during onset of the acute phase of the disease. Unfortunately, however, drug efficacy diminishes with time since infection and 40% of patients suffer from adverse effects due to treatment (WHO 2017). Hence, new drugs with improved safety and efficacy are needed.

Sleeping Sickness, which is also known as Human African trypanosomiasis or HAT, is caused by two subspecies of *T. brucei* (*T. b. gambiense* and *T. b. rhodesiense*) that are transmitted predominantly through the bite of an infected tsetse fly. In the first stage of the disease, parasites multiply in subcutaneous tissues, blood and lymph, before crossing the blood-brain barrier and infecting the central nervous system in the second stage of the disease. Without treatment, sleeping sickness is invariably fatal (WHO 2017). Currently, five drugs, each with undesirable side effects, are available for the treatment of sleeping sickness, and the stage of the disease dictates which should be administered. As for Chagas disease, early treatment provides better prospects for a cure. Unfortunately, the drugs required to treat the second stage of the disease are challenging to administer and/or toxic (and, in some cases, lethal) (WHO 2018c). Hence, although the incidence of sleeping sickness has been declining due to sustained control efforts, and in 2017 there were just 1447 new cases (WHO 2018d), there is a need for safe and effective new drugs.

As illustrated in the examples highlighted below, fragment-based approaches have been utilized in several antitrypanosomal drug discovery projects spanning more than two decades. They have revealed binding hot spots and previously unidentified binding pockets, provided chemical starting points for novel inhibitors (only some of which have been pursued), and facilitated optimization of antitrypanosomal HTS hits.

Targeting the peroxin 5-peroxin 14 interaction using a fragment-guided approach

Trypanosomes and other kinetoplastids uniquely possess a membrane-bound, peroxisomal-like organelle known as a glycosome, in which glucose metabolism and other metabolic reactions occur (Haanstra et al. 2016). Biogenesis of this organelle depends on proteins called peroxins or PEX. For example, the import receptor PEX5 mediates import of glycosomal enzymes from the cytoplasm into the organelle through a process dependent on an interaction with the N-terminus of PEX14, a glycosomal-membrane associated protein (Haanstra et al. 2016). After determining the solution NMR structure of the N-terminal domain of *T. brucei* PEX14 (*Tb*PEX14) that interacts with the intrinsically-disordered N-terminus of PEX5, Dawidowski et al. (2017) embarked on an *in silico* screen of a subset of the ZINC library. In doing so,

they identified a pyrazolo[4,3-*c*]pyridine derivative (**1**, Figure 1) that binds the N-terminus of PEX14 with modest affinity, disrupts its interaction with PEX5 (K_i = 61.6 μM, LE = 0.19), and kills blood-stage *T. brucei* (EC_{50} = 21 μM) more effectively than mammalian cells. The authors thereafter used a fragment-based approach to facilitate optimization of this inhibitor. To guide the design of inhibitors with improved affinity, they screened an in-house library of 1500 fragments (initially in cocktails of five, each at a concentration of 1 mM) for binding to ^{15}N-labeled PEX14 using ^{1}H-^{15}N-Heteronuclear Multiple-Quantum Correlation (HMQC) NMR. This screen yielded twelve fragments binding with K_D values below 2 mM and revealed a tendency of the protein to bind fused bicyclic aromatic ring systems (Table 1). This in turn led the researchers

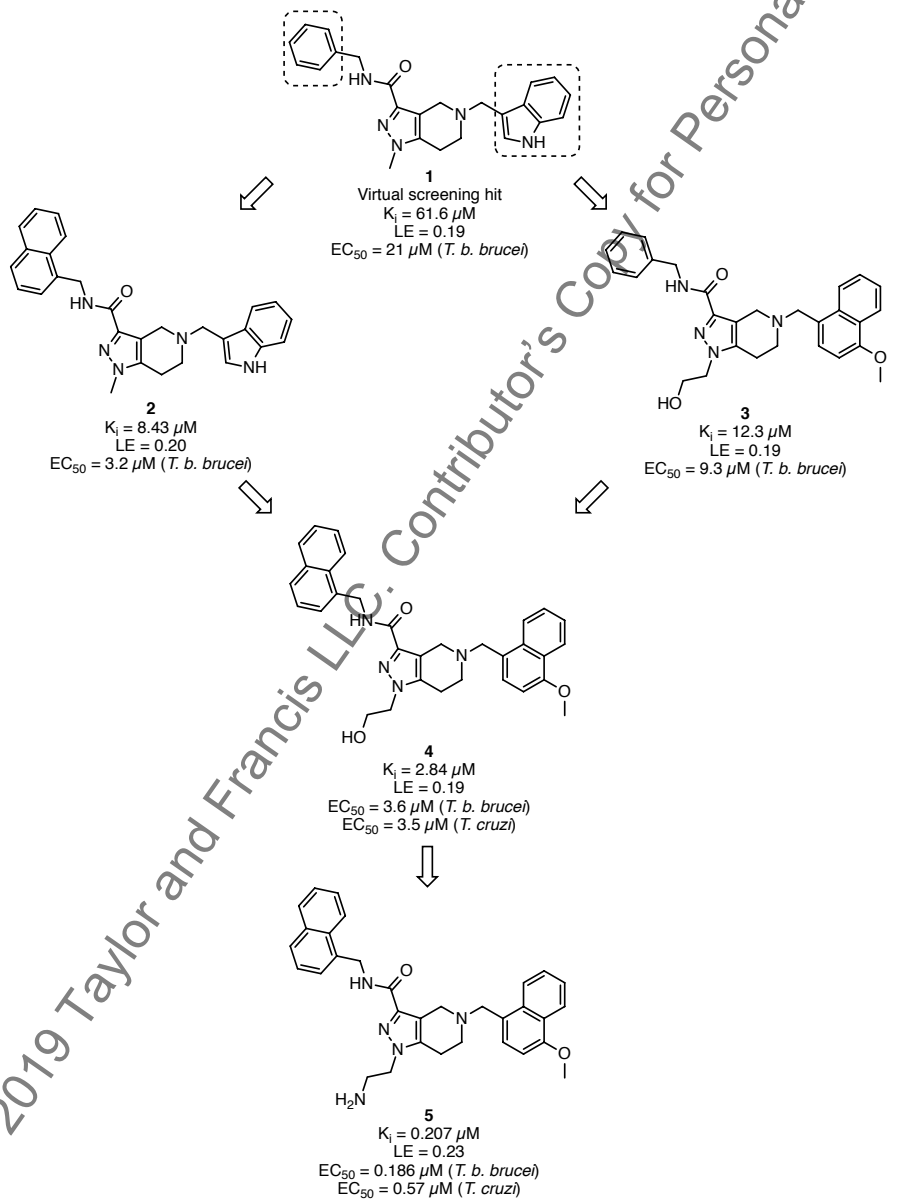

Figure 1. Fragment-guided optimization of an inhibitor of the interaction between *T. brucei* PEX14 and PEX5 identified in a virtual screen. Terminal aromatic moieties of virtual screening hit **1** (dashed rectangles) were replaced with naphthyl moieties, a common scaffold among the fragment hits (Table 1). K_i, inhibition constant; LE, ligand efficiency = (−RTln(K_i))/NHA, in kcal.mol^{-1}.NHA^{-1}; EC_{50}, half maximal effective concentration as measured in whole-cell assays.

Table 1. Examples of fragment-based approaches applied to antitrypanosomal drug discovery.

Target	Approach	Selected fragment hit(s)	Elaborated compound(s)	Reference
*Tb*PEX14-PEX5	Fragment-guided optimization. ^{1}H-^{15}N-HMQC-based screen of 1500 fragments performed	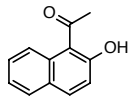 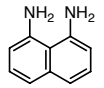 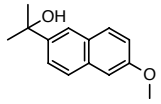	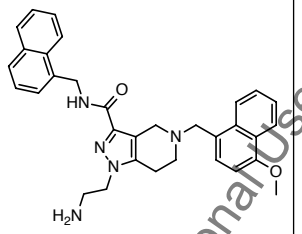 **5** [a]K_i = 0.207 µM [b]LE = 0.23 [c]EC_{50} (*T. b. brucei*) = 0.186 µM EC_{50} (*T. cruzi*) = 0.57 µM	Figure 1 Dawidowski et al. (2017)
*Tc*SpdSyn	DSF and SPR-based fragment screen, followed by enzyme assay and X-ray crystallography	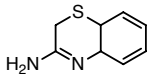 [d]IC_{50} = 180 µM LE = 0.46 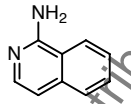 IC_{50} = 460 µM LE = 0.41 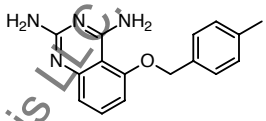 IC_{50} = 9.1 µM LE = 0.33 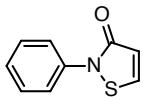 IC_{50} = 0.051 µM LE = 0.83	N/A	Amano et al. (2015)

Table 1 contd. ...

...Table 1 contd.

Target	Approach	Selected fragment hit(s)	Elaborated compound(s)	Reference
*Tb*PDEB1	Enzyme assay (luminescence-based) screen of 1040 fragments followed by whole-cell tests	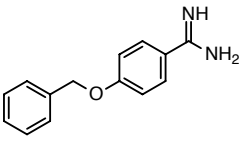 IC_{50} = 50 µM LE = 0.34 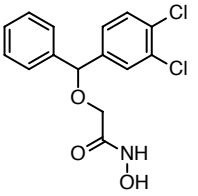 IC_{50} = 12.5 µM LE = 0.32 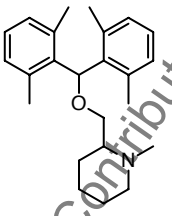 IC_{50} = 63 µM LE = 0.22 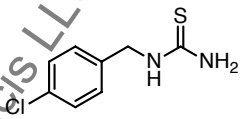 IC_{50} = 100 µM LE = 0.45	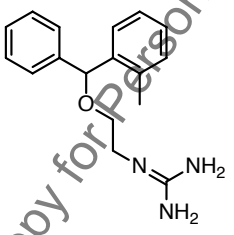 [a]IC_{50} (parasite) = 2.0–7.9 µM 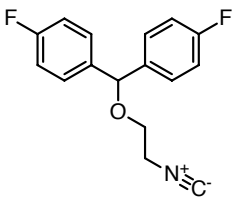 IC_{50} (parasite) = 0.2–63 µM	Blaazer et al. (2015)
	Fragment growing guided by scintillation proximity assay data	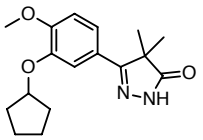 **6** IC_{50} = 12 µM LE = 0.30	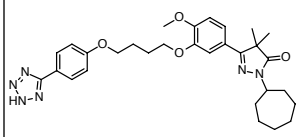 **14** IC_{50} (*Tb*PDEB1)= 49 nM IC_{50} (*T. brucei*) = 520 nM LE = 0.25	Figure 2 Orrling et al. (2012)

Table 1 contd. ...

...Table 1 contd.

Target	Approach	Selected fragment hit(s)	Elaborated compound(s)	Reference
*Tc*HisRS	X-ray crystallography-based screen of 680 fragments, followed by DSF and aminoacylation assay. Fragment growing and tethering	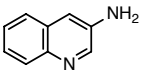 **15** IC_{50} > 2 mM LE < 0.33	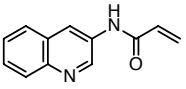 **18** IC_{50} = 0.85 mM LE = 0.28 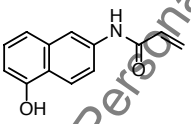 **19** IC_{50} = 1.65 mM LE = 0.24	Figure 3 Koh et al. (2015)
Rhodesain	Fragment tethering. Enzyme assay-based screen of 200 cysteine-reactive fragments	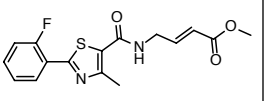 $^{f}k_{inact}/K_i$ = 18.3 $M^{-1}.s^{-1}$ IC_{50} (*T. brucei*) = 30 µM 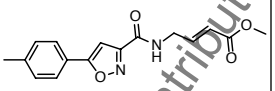 K_{inact}/K_i = 13.2 $M^{-1}.s^{-1}$ IC_{50} (*T. brucei*) = 43 µM	N/A	McShan et al. (2015)
*Tb*RFK	Ultrafiltration-based screen of 134 fragments	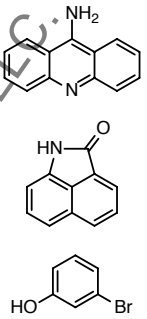	N/A	Shibata et al. (2011)
^{g}*Tb*REL1	*In silico* (CrystalDock) fragment hit identification and fragment-assisted optimization	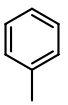	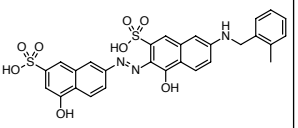	Durrant et al. (2011)

Table 1 contd. ...

...Table 1 contd.

Target	Approach	Selected fragment hit(s)	Elaborated compound(s)	Reference
*Tb*PTR1	Virtual screen of 26,084 fragments. Prioritized fragments tested in enzyme assay	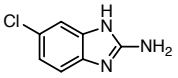 **20** $^{h}K_i^{app}$ = 10.6 μM LE = 0.62	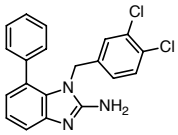 **23** K_i^{app} = 0.007 μM LE = 0.44 EC_{50} = 10 μM	Figure 4 Mpamhanga et al. (2009), Spinks et al. (2011)
*Tb*6PGDH	Virtual screen of 64,000 fragments. Prioritized fragments tested in enzyme assay	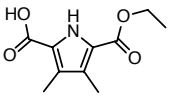 IC_{50} = 45 μM LE = 0.40 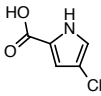 IC_{50} = 43 μM LE = 0.66 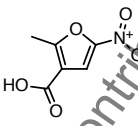 IC_{50} = 28 μM LE = 0.52	N/A	Ruda et al. (2010)
*Tb*NDRT	X-ray crystallographic fragment screen of 304 fragments	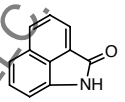 EC_{50} (*T. brucei*) = 0.12 mM 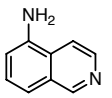 EC_{50} (*T. brucei*) = 0.25 mM 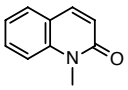 EC_{50} (*T. brucei*) = 0.41 mM 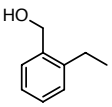 EC_{50} (*T. brucei*) = 1.3 mM	N/A	Verlinde et al. (2009), Bosch et al. (2006)

[a]K_i, inhibition constant; [b]LE, ligand efficiency = $(-RT\ln(K_D/K_i/IC_{50}))$/NHA, in kcal.mol^{-1}.NHA^{-1}; [c]EC_{50}, half maximal effective concentration as measured in whole-cell assays; [d]IC_{50}, concentration causing 50% inhibition as measured in enzyme assays, unless otherwise specified; [e]Range of IC_{50} values measured in whole-cell assays against *T. brucei*, *T. cruzi*, *L. infantum*, *P. falciparum*; [f]k_{inact}, rate of inactivation; [g]Compounds shown in the *Tb*REL1 row are *in silico* predicted binders. Binding has not been experimentally confirmed; [h]K_i^{app}, the apparent value of K_i.

to introduce naphthyl substituents in place of two terminal aromatic moieties that were predicted by docking to bind in adjacent hydrophobic cavities that accommodate two aromatic residues of PEX5. Introduction of one or two naphthyl moieties improved inhibitory activity in an AlphaScreen-based competition assay (K_i = 8.4 or 12.3 μM for compounds **2** and **3**, respectively, each with a single naphthyl substituent, or 2.8 μM for compound **4**, which has two naphthyl moieties) and also enhanced trypanocidal activity (EC_{50} = 3.2 and 9.3 μM for compounds **2** and **3**, respectively, or 3.6 μM for compound **4**) (Figure 1). X-ray crystal structures of the optimized inhibitors showed that the naphthyl rings filled the hydrophobic pockets as intended. Replacement of a hydroxyl moiety of compound **4** with an amine, produced compound **5**, which inhibits the PEX14-PEX5 interaction with a K_i of 207 nM (LE = 0.23) and demonstrates antitrypanocidal activity against *T. b. brucei*, *T. b. rhodesiense* and the intracellular amastigote form of *T. cruzi* with EC_{50} values of 0.186, 0.021 and 0.57 μM, respectively. Key differences between the N-termini of PEX14 from trypanosomes and humans were considered during inhibitor design and, favorably, compound **5** shows selectivity for trypanosomal PEX14 over the human variant (IC_{50} (*T. brucei* PEX14) = 1.34 μM vs IC_{50} (human PEX14) = 37.8 μM), and lower toxicity against mammalian cell lines tested.

Dawidowski et al. (2017) went on to show that in the presence of compound **5**, glycosomal enzymes mislocalize to the cytosol and trypanosomal ATP levels are reduced as was predicted if hexokinase and phosphofructokinase mislocalize, and glucose phosphorylation is, as a consequence, unregulated. These data, and the observed correlation between affinity for PEX14 and antitrypanosomal activity for the pyrazolo[4,3-*c*]pyridine derivatives tested, are consistent with the antitrypansomal activity of the PEX14-PEX5 inhibitors being on target, and hence validate PEX5-PEX14 as a trypanosomal drug target. Following modification of the lead PEX5-PEX14 inhibitor to reduce plasma protein binding, antitrypanosomal activity could be observed also in a murine model of HAT. A reduction in parasitemia, with no adverse effects on the mice, was observed when the compound was administered at 100 mg/kg twice a day for five days. Further optimization of absorption, distribution, metabolism and excretion (ADME) properties is expected to yield a clinical candidate.

Targeting spermidine synthase

Trypanothione is a bis(gluthionyl)-spermidine conjugate essential for, and unique to, kinetoplastids such as trypanosomes and leishmania (Fairlamb et al. 1985). It functions to protect the cells from oxidative stress (Krauth-Siegel and Comini 2008). In light of the parasites' requirement for trypanothione, the enzymes involved in its biosynthesis—including spermidine synthase, which catalyses the conversion of putrescine to spermidine—have attracted attention as potential antiparasitic drug targets (Birkholtz et al. 2011). Using a fragment-based approach, Amano et al. (2015) set out to identify novel inhibitors of *T. cruzi* spermidine synthase (*Tc*SpdSyn). In order to target the putrescine binding site of *Tc*SpdSyn, rather than the pocket that tightly binds the decarboxylated *S*-adenosyl-L-methionine (dcSAM) also required for the reaction, fragment screening was performed in the presence of dcSAM. In their approach, fragments were screened both by differential scanning fluorimetry (DSF; at a concentration of 2 mM) and surface plasmon resonance (SPR; at a concentration of 250 μM). Fragments observed to stabilize the protein to thermal-denaturation in the DSF assay and/or bind the protein in the SPR assay were selected for *Tc*SpdSyn crystal soaking experiments and evaluation of inhibitory activity in an enzyme assay. Amano et al. (2015) describe co-crystal structures of six fragments identified in the screen. Two of the fragment hits were observed to bind the putrescine-binding pocket, interacting with both the protein and bound dcSAM. These fragments inhibit the enzyme with IC_{50} values of 180 and 460 μM, corresponding to LE values of 0.46 and 0.41, respectively (Table 1). Interestingly, the remaining four fragment hits were observed to bind at the interface of the two monomers in the *Tc*SpdSyn dimer, with one fragment binding covalently. All four of the interface-binding fragments inhibit the enzyme allosterically. The most potent of the non-covalently bound fragments binding at the interface inhibits the enzyme with an IC_{50} value of 9.1 μM (LE = 0.33), and the covalently bound fragment, which was observed to bind twice (forming disulfide bonds with Cys239 of each monomer) inhibits *Tc*SpdSyn with an IC_{50} value of 0.051 μM (LE = 0.83) (Table 1). This study not only identified ligand efficient fragments that could serve as starting points for novel *Tc*SpdSyn inhibitors, but also revealed two binding sites, including an allosteric site composed of

residues not conserved between *Tc*SpdSyn and its human orthologue, that could be exploited for further structure-based design of selective *Tc*SpdSyn inhibitors.

Targeting 3',5'-cyclic nucleotide phosphodiesterase

Cyclic nucleotide phosphodiesterases (PDEs) play a key role in regulating levels of cyclic nucleotides in cells through hydrolysis of the phosphodiester bond of cAMP and/or cGMP. Two 3',5'-cyclic nucleotide phosphodiesterases (PDEB1 and B2, which are 76.2% similar to each other) have been shown using RNAi (Oberholzer et al. 2007), as well as with a small molecule inhibitor (de Koning et al. 2012), to be essential for proliferation of *T. brucei in vitro* and *in vivo* when knocked down together. Two distinct fragment-based approaches targeting these enzymes have been published.

Blaazer et al. (2015) screened a commercially available library of 1040 fragments (with slightly higher molecular weight and complexity than a rule-of-three compliant fragment library) against *T. brucei* PDEB1 (*Tb*PDEB1) using a luminescence-based biochemical assay. In parallel, fragments were tested against a human PDE (PDE4D) in order to facilitate prioritization of fragment hits selective for the parasite enzyme. A set of twelve fragments that inhibit *Tb*PDEB1 by more than 90% at a concentration of 200 μM was identified in the screen, as was a set of seven fragments that show selectivity for *Tb*PDEB1 over human PDE4D. Blaazer et al. (2015) focused on a set of four fragment hits (Table 1) that shared similarity with the scaffolds of known drugs. These fragments, along with analogues of each chosen from in-house libraries of drug-like compounds, were then tested for whole-cell activity against a panel of parasites (*T. brucei*, *T. cruzi*, *Leishmania infantum* and *Plasmodium falciparum*) as well as human cells. The two fragment hits with the highest molecular weight (which share a biphenyl core) showed antiparasitic activity against multiple parasites, as did a number of analogues. Two analogues (Table 1) with improved antiparasitic activity (meeting or surpassing that of benznidazole and miltefosine against *T. cruzi* and *L. infantum*, respectively) and selectivity are under further investigation (Blaazer et al. 2015). Whether the antiparasitic effect of these compounds is a consequence of PDE inhibition remains to be reported.

Orrling et al. (2012) identified a catechol pyrazolinone fragment (compound **6**, Figure 2a) that inhibits *Tb*PDEB1 with an IC_{50} value of 12 μM (LE = 0.30) in a follow up of chemotypes related to a HTS hit (compound **7**, Figure 2b; IC_{50} (*Tb*PDEB1) = 4 nM, LE = 0.27, IC_{50} (*T. brucei*) = 80 nM) (Orrling et al. 2012). The fragment carries multiple structural features present in known inhibitors of *T. brucei* (compound **8**, Figure 2b) or human PDEs (compounds **9** and **10**, Figure 2b), enzymes that have been extensively studied as drug targets for human diseases. Orrling et al. (2012) performed docking experiments with a homology model of *Tb*PDEB1 based on the structure of *Leishmania major* PDEB1 (which shares 66% sequence identity), to predict how the fragment and related human PDE inhibitors bind the enzyme. Based on docking poses, the researchers identified two opportunities for growth of the fragment—from the pyrazolinone nitrogen, and through replacement of the cyclopentyl ring, which was positioned at the entrance to a parasite-specific pocket named the P-pocket. Growth of the fragment from the pyrazolinone nitrogen through introduction of an aliphatic substituent (namely a cycloheptyl moiety) increased potency against *Tb*PDEB1 in a scintillation proximity assay (IC_{50} = 0.41 μM, LE = 0.30); however, this molecule (compound **11**, Figure 2c), like the parent fragment, lacked whole-cell activity. Replacement of the cyclopentyl moiety with a benzyl moiety increased the potency against the enzyme just twofold (compound **12**, IC_{50} = 6.3 μM, LE = 0.30) but, encouragingly, conferred activity against the parasite (IC_{50} = 8.6 μM). Furthermore, introduced together, as in compound **13**, these two modifications yielded an inhibitor with IC_{50} values of 0.5 μM (LE = 0.28) and 6.3 μM against the enzyme and parasite, respectively. Encouragingly, compound **13** was without effect on a human fibroblast cell line at the concentrations tested. Further chemical synthesis was focused on growing the molecule to pick up interactions in the P-pocket. Inspired by the structure of HTS hit **7**, a butyloxy linker was introduced between the phenyl moieties and a tetrazole substituent was introduced (compound **14**). This increased the potency against both *Tb*PDEB1 and *T. brucei* (IC_{50} = 0.049 μM (LE = 0.25) and 0.52 μM, respectively). Although the compound was also a potent inhibitor of a panel of human PDEs it showed selectivity at the whole-cell level (IC_{50} (human fetal lung fibroblasts) > 64 μM). Orrling et al. (2012) additionally presented evidence that the antitrypanosomal activity of the final compound was indeed a consequence of PDE inhibition; the compound was shown

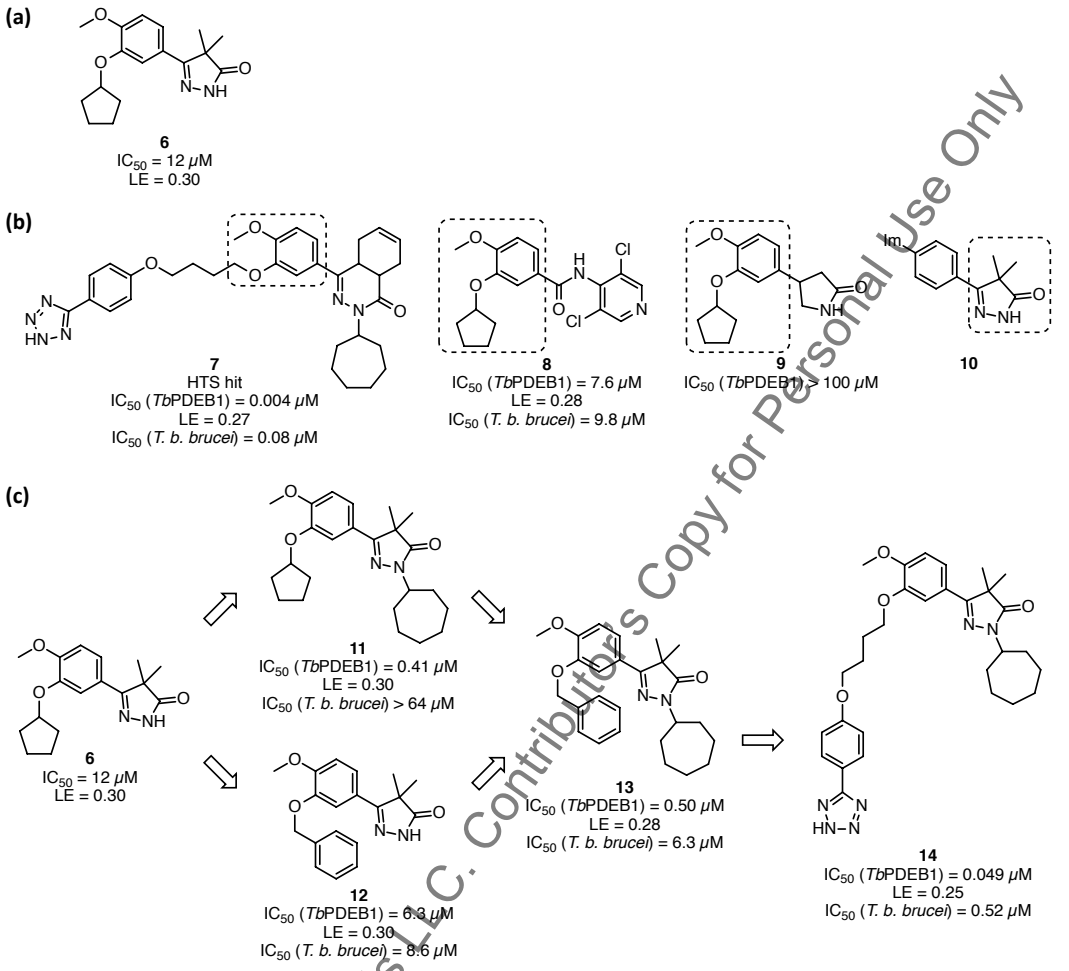

Figure 2. Fragment growth in the development of *Tb*PDEB1 inhibitors. Fragment hit **6 (a)**, which shares key features of HTS hit **7** and other known *Tb*PDEB1 (compound **8**) or human PDE (**9** and **10**) inhibitors **(b)**, was shown to inhibit *Tb*PDEB1. Dashed rectangles highlight common structural features. Fragment **6** was elaborated using a fragment growing strategy **(c)**. IC_{50} values for inhibition of *Tb*PDEB1 activity or *T. b brucei* proliferation are shown. LE, ligand efficiency = $(-RT\ln(IC_{50}(TbPDEB1)))/NHA$, in $kcal.mol^{-1}.NHA^{-1}$.

to (i) increase cAMP levels in an engineered trypanosome strain with a FRET-based cAMP sensor, and (ii) cause phenotypic changes (formation of duplicate/multiple nuclei and kinetoplasts) consistent with changes observed following genetic or chemical knock-down of *Tb*PDEs (Oberholzer et al. 2007, de Koning et al. 2012).

Targeting histidyl-tRNA synthetase using a fragment-tethering approach

Aminoacyl-tRNA synthetases are well-validated parasite drug targets (Kalidas et al. 2014, Pham et al. 2014). Having previously solved X-ray crystal structures of *T. cruzi* histidyl-tRNA synthetase (*Tc*HisRS), *T. brucei* HisRS, and human cytosolic HisRS (Merritt et al. 2010, Koh et al. 2014), and identified trypanosomal-specific pockets (Koh et al. 2014), Koh et al. (2015) sought to identify chemical starting points for parasite-selective HisRS inhibitors by performing an X-ray crystallographic fragment screen of the Medical Structural Genomics of Pathogenic Protozoa (MSGPP) fragment library. Histidine-complexed

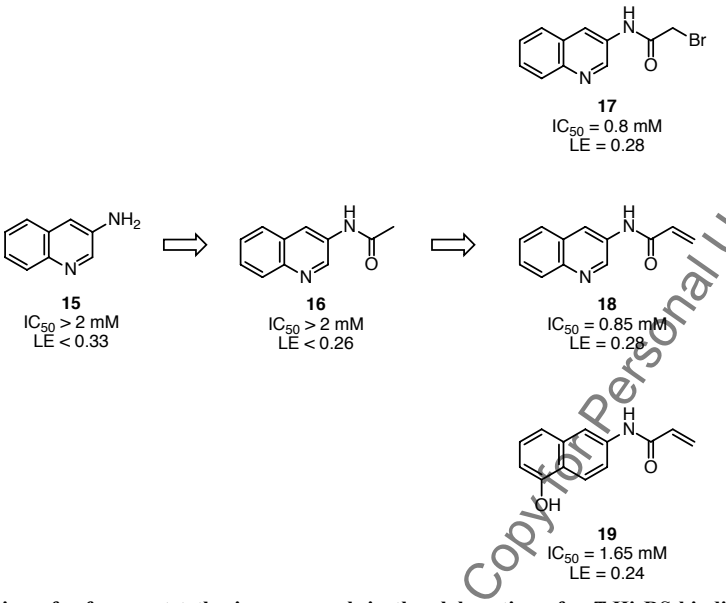

Figure 3. Application of a fragment tethering approach in the elaboration of a *Tc*HisRS-binding fragment hit. IC_{50} values measured in an aminoacylation assay are shown. LE = (−RTln(IC_{50}))/NHA, in kcal.mol^{-1}.NHA^{-1}.

*Tc*HisRS crystals were soaked with 68 different fragment cocktails of ten fragments each. Co-crystal structures were solved for fifteen fragments (2.2% hit rate), and all fifteen fragments were observed to bind to the same site—a narrow groove adjacent to the histidine binding site that is not present in the crystal structure without the fragments bound. The site is in very close proximity to the binding site of the adenine ring of the histidyl-AMP reaction intermediate and it is likely that fragment binding will interfere with ATP/histidyl-AMP binding. Although fragment binding was observed by X-ray crystallography, binding of only one of the fifteen fragments could be detected by DSF, when fragments were tested at 1 mM. Additionally, the fragments showed little inhibitory activity in an aminoacylation assay; at a concentration of 2 mM, the most active fragments (including the fragment that gave rise to a thermal shift in the DSF assay) inhibited aminoacylation by 20–39%.

With detailed knowledge of the fragment binding mode, Koh et al. (2015) attempted to grow fragment hit **15** (Table 1, Figure 3). Three analogues with substituents on the 3-amino group, intended to extend the fragment toward the histidine binding site, were synthesized (e.g., compound **16**, Figure 3). A co-crystal structure of *Tc*HisRS with compound **16** (which showed similar inhibitory activity to the parent fragment) was obtained, but interestingly it revealed that the substituent caused the fragment to flip in the binding site. The researchers took advantage of the finding that the substituent (an acetamide moiety) was now in close proximity to a cysteine residue (Cys365) not present in the human enzyme, and in a fragment tethering approach synthesized reactive fragments with an electrophile introduced (compounds **17–19**, Figure 3). Co-crystal structures were obtained for two of the three reactive fragments (compounds **18** and **19**, both with acrylamide moieties replacing the acetonide group) and these showed the fragments to bind as intended, with the electron density around the acrylamide group consistent with covalent bond formation. Although these compounds did not increase the melting temperature of the protein by DSF, they did show improved and selective activity in the aminoacylation assay (IC_{50} = 0.85 and 1.65 mM against *Tc*HisRS vs IC_{50} >2 mM against human cytosolic and mitochondrial HisRS; Table 1, Figure 3).

Targeting rhodesain with reactive fragments

Rhodesain, a major cathepsin L-like cysteine protease, is required for survival of *T. b. rhodesiense* (Steverding et al. 2012, Ettari et al. 2013). Furthermore, the *T. cruzi* homologue of rhodesain (cruzain) is

the target of a drug candidate that has progressed to late-stage preclinical development (K777; McKerrow et al. 2009). McShan et al. (2015) recently screened a library of 200 cysteine-reactive electrophilic fragments against rhodesain using a biochemical assay. Two fragments that reproducibly inhibit the protease by ≥ 85% at a concentration of 10 μM were identified (Table 1). Encouragingly, the fragments also possess antitrypanosomal activity (IC_{50} (*T. brucei*) = 30 and 43 μM) and demonstrate selectivity (IC_{50} (Hep G2) > 150 μM).

Targeting riboflavin kinase using an ultrafiltration-based fragment screen

To validate an ultrafiltration-based fragment screening approach, Shibata et al. (2011) screened a library of 134 fragments against *T. brucei* riboflavin kinase (*Tb*RFK). From 134 fragments screened in 23 cocktails, each containing five to nine fragments, three fragment hits were identified (Table 1). Subsequent competitive binding assays revealed that flavin mononucleotide (FMN) decreased binding of each of the fragments, while ADP-Mg increased binding. These observations are consistent with the fragments binding in the FMN binding site, which is reported to be stabilized upon ADP-Mg binding (Bauer et al. 2003, Karthikeyan et al. 2003).

In silico *fragment-assisted optimization of an inhibitor of RNA editing ligase 1*

To demonstrate the utility of CrystalDock, an algorithm designed to identify fragments likely to bind a protein pocket, Durrant et al. (2011) used the algorithm to identify fragments likely to bind to the adenylation domain of *T. brucei* RNA editing ligase 1 (*Tb*REL1). The algorithm identified three clusters of fragments likely to bind in the *Tb*REL1 active site. One cluster of hydrophobic fragments was interestingly predicted to bind in close proximity to the predicted binding site of a low-μM naphthalene-based inhibitor (Durrant et al. 2010), in a small pocket not previously exploited for drug discovery. This presented the opportunity to improve the affinity of the naphthalene-based inhibitor through fragment linking. One of the hydrophobic fragments—a toluene fragment (Table 1)—was positioned such that it could be linked via a methylene linker to the inhibitor. Subsequent binding energy calculations are consistent with the elaborated inhibitor (Table 1) binding with higher affinity; however, this needs to be experimentally validated.

Targeting PTR1

Tryanosomes require pterin for growth, yet lack enzymes for its *de novo* synthesis, rendering the parasites dependent on the salvage of oxidized pteridines, such as biopterin, and their subsequent reduction by pteridine reductase (PTR1). Following the demonstration that *T. brucei* PTR1 (*Tb*PTR1) is required for survival of blood stage *T. brucei* parasites *in vitro* (Sienkiewicz et al. 2010), Mpamhanga et al. (2009) set out to validate *Tb*PTR1 chemically and identify leads for novel HAT drugs. The need to identify novel *Tb*PTR1 inhibitors was a primary factor that motivated the use of a fragment-based approach; many existing PTR1 inhibitors were derived from dihydrofolate reductase (DHFR) inhibitors, and also inhibit human and *T. brucei* DHFR. Such activity would render any *Tb*PTR1 inhibitor unsuitable for use as a chemical probe or drug lead. Furthermore, existing inhibitors, which primarily have a 2,4-diaminopteridine, 2,4-diaminoquinazoline, or 2,4-diaminopyrimidine core (Figure 4a), have relatively high polar surface areas (PSAs: 77–100 Å^2), which is an undesirable property of a lead required to permeate the blood-brain barrier. A second key factor in choosing a fragment-based approach was the availability of multiple *Tb*PTR1 (and *L. major* PTR1) X-ray crystal structures, which showed a well-defined binding cleft.

The fragment-based approach used to target *Tb*PTR1 began with an *in silico* screen of 26,084 fragment-like compounds against a representative *Tb*PTR1 crystal structure. The fragment library, which was derived from a database of lead-like compounds filtered to retain only compounds with < 20 heavy atoms, ≤ 2 ring systems, at least one hydrogen-bond donor, < 4 rotatable bonds and a clogP or clogD < 3.5, was docked into the active site of *Tb*PTR1. A set of 2725 compounds predicted to interact with the

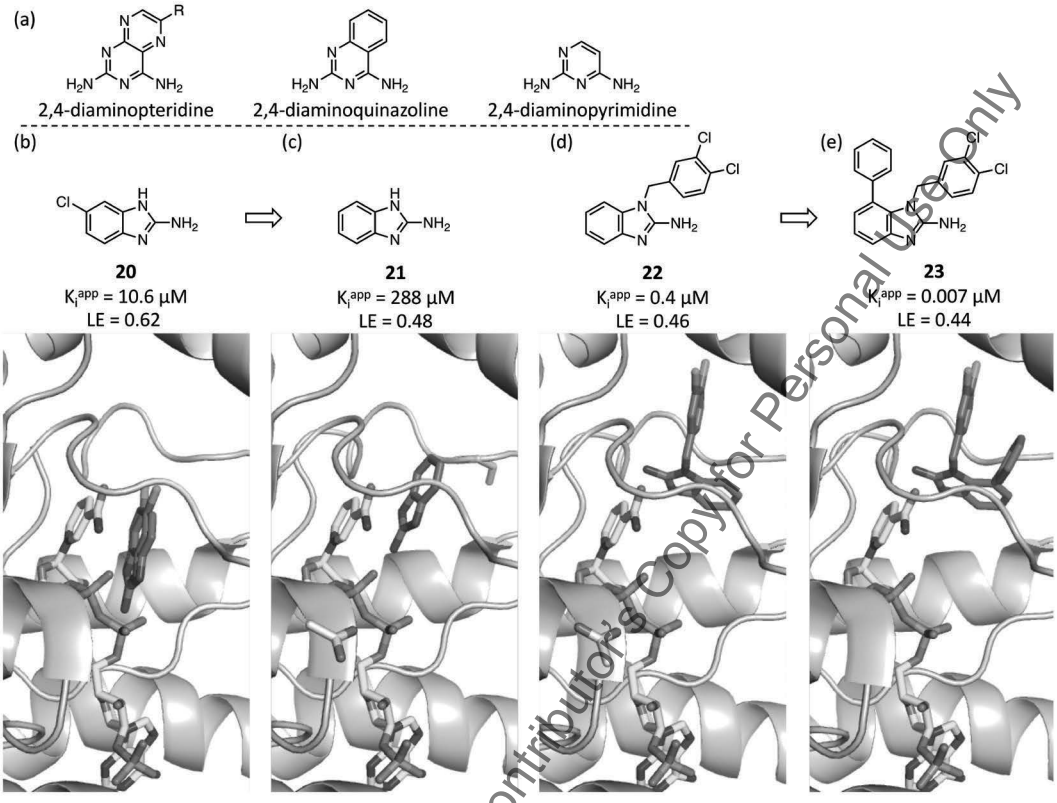

Figure 4. Fragment-based approach to identifying novel inhibitors targeting *Tb*PTR1. (a) Common scaffolds of known PTR1 and DHFR inhibitors. **(b)** Crystal structure showing binding of an aminobenzimidazole fragment hit (carbons in magenta) identified in a virtual fragment screen, to *Tb*PTR1 (with bound $NADP^+$ cofactor, carbons in yellow) [PDB ID: 2WD7]. The fragment was observed to bind in two overlapping poses. **(c–e)** Crystal structures of analogues of fragment **20** in complex with *Tb*PTR1-$NADP^+$ [PDB IDs: 3GN1, 3GN2, 2WD8]. An acetate molecule (carbons in grey) can be seen in the crystal structures shown in (c) and (d). LE = $(-RT\ln(K_i^{app}))/NHA$, in $kcal.mol^{-1}.NHA^{-1}$.

Color version at the end of the book

β-phosphate of the enzyme's $NADP^+$ cofactor and participate in additional hydrogen bonding interactions observed in previously obtained inhibitor-complexed *Tb*PTR1 crystal structures, were prioritized for further analysis. Following removal of compounds containing scaffolds of known PTR1 inhibitors and consideration of (i) scaffold diversity, (ii) PSA of the scaffolds (ideally to be < 70 A^2), (iii) results of minimization, and (iv) shape complementarity with the binding site, the researchers arrived at a list of 59 compounds, 45 of which were commercially available. These compounds were purchased and three fragments were shown to inhibit *Tb*PTR1 by more than 50%, and a further seven between 30 and 50%, in a biochemical assay.

Although Mpamhanga et al. (2009) were unable to co-crystallize the aminobenzothiazole fragment with the second highest activity (K_i^{app} = 21 μM, LE = 0.46), they did obtain a co-crystal structure of the aminobenzimidazole fragment with the highest activity (compound **20**, Figure 4b and Table 1; K_i^{app} = 10.6 μM, LE = 0.62) bound to *Tb*PTR1 (Figure 4b). Interestingly, the ligand was found to adopt two distinct binding poses, both of which involved hydrogen bonding with the phosphate moiety of $NADP^+$, and the predominant pose was in close agreement with the highest scoring docking pose. Co-crystal structures of two closely related aminobenzimidazole fragments (compounds **21** and **22**) were also obtained but interestingly, despite sharing an aminobenzimidazole core, the fragments adopted distinct binding poses (Figures 4c and d). Compound **22**, the more potent of the two analogues (with a K_i^{app} an order of

magnitude lower than the original fragment hit; K_i^{app} = 0.4 μM), was observed to bind 3.7 Å away from the nicotinamide moiety of $NADP^+$ and to not form any hydrogen bonds with the cofactor. The co-crystal structure revealed hydrophobic pockets adjacent to the aminobenzimidazole core and in an attempt to improve the affinity of compound **22**, derivatives with substituents introduced to fill the largest pocket were tested. This ultimately produced aminobenzimidazole derivative **23**, which inhibits *Tb*PTR1 with a K_i^{app} of 7 nM (Table 1, Figure 4e). This time a co-crystal structure showed that the binding mode of the aminobenzimidazole was maintained. Favorably, none of the *Tb*PTR1 inhibitors identified showed appreciable activity against human or *T. brucei* DHFR as hoped, and the lead aminobenzimidazole has physicochemical properties suitable for cell and CNS penetration (molecular weight of 368 Da, PSA of 55 Å, and logD of 3.7). However, disappointingly, the EC_{50} measured against *T. brucei* in cell culture was 10 μM, over a thousand fold higher than the K_i^{app} measured against the enzyme. Based on the results of knock-down and additional kinetic studies, it seems likely that to see the level of antitrypanosomal activity required in a drug candidate, potency against PTR1 will need to be increased by at least two orders of magnitude (Spinks et al. 2011).

Targeting 6-phosphogluconate dehydrogenase

Ruda et al. (2010) used a similar *in silico* fragment screening approach to that used against PTR1, to target 6-phosphogluconate dehydrogenase of *T. brucei* (*Tb*6PGDH). This essential pentose phosphate pathway enzyme (Hanau et al. 2004) catalyzes the oxidative decarboxylation of 6-phosphogluconate (a molecule with phosphate, carboxylate and hydroxyl groups) and, as a consequence, has an active site composed of several polar residues. Potent and selective substrate-like inhibitors of the enzyme have been reported, but they lack trypanocidal activity (e.g., Dardonville et al. (2004)), presumably due to poor cellular permeability resulting from their charge and polarity.

In this study, a library of 64,000 fragments was compiled from the available chemicals and screening compounds directories (ACD-SCD). Compounds were required to be < 320 Da in size and possess a phosphonate, sulfonate, sulfonic acid, sulfonamide, carboxylic acid or tetrazole to mimic the phosphate group of known inhibitors. The inclusion of such functional groups was anticipated to facilitate binding to the positively charged site that accommodates the phosphate of 6-phosphogluconate but produce less polar starting points for drug discovery compared with the known phosphate-containing inhibitors. Although the crystal structure of *Tb*6PGDH had been solved, the structure of *Lactococcus lactis* 6PGDH was used as the template for docking because of the availability of cofactor, substrate and inhibitor co-crystal structures. Substrate-binding residues are fully conserved between the two proteins. The docking approach involved placement of the phosphate isosteres in the phosphate binding site, and was first validated by docking of known inhibitors. Binding modes were predicted for 5836 of the 64,000 fragments, and following clustering and visual inspection of the predicted binding poses of high-scoring compounds, a set of 71 fragments was purchased and tested against *Tb*6PGDH in a biochemical assay. Ten compounds showed > 80% inhibition when tested at a concentration of 200 μM, and IC_{50} values below 50 μM were determined for three 5-membered carboxylic acid-containing heterocycles among these (corresponding to LEs of 0.40–0.66; Table 1). Fifty-three analogues of the initial ten hits were purchased, leading to the identification of a further three compounds with IC_{50} values below 50 μM and LEs between 0.48 and 0.60, albeit with two showing hill slopes ≥ 2, possibly indicative of non-specific inhibition. Pending structural validation of the proposed binding modes, the inhibitory fragments—invariably 5-membered heterocycles containing a carboxylic acid as a phosphate replacement—provide ligand efficient chemical starting points for the development of novel *Tb*6PGDH inhibitors. With higher partition coefficients, lower total PSAs and predicted improved human intestinal absorption, the fragments have the potential to yield more drug-like inhibitors than those identified previously.

Targeting nucleoside 2-deoxyribosyltransferase

Nucleoside 2-deoxyribosyltransferase functions in the nucleoside salvage pathway, catalyzing the transfer of deoxyribose between nucleobases. As *T. brucei* lacks the enzymes required for *de novo* purine synthesis and

is dependent on purine nucleoside scavenging, the enzyme was proposed as a potential drug target (Bosch et al. 2006). This enzyme is particularly attractive as a target because humans are devoid of nucleoside 2-deoxyribosyltransferases (and instead rely on purine and pyrimidine phosphorylases), and as such it should be possible to design inhibitors that selectively target the pathogen. After solving the X-ray crystal structure of *T. brucei* nucleoside 2-deoxyribosyltransferase (*Tb*NDRT) in the *apo* form (to 1.8 Å), Bosch et al. (2006) performed an X-ray crystallographic fragment screen against the enzyme.

In the screen, *Tb*NDRT crystals were soaked with 304 fragments (an earlier version of the fragment library screened against *Tc*HisRS) in 31 different cocktails of approximately 10 fragments each. Four fragments (Table 1), as well as glycerol (originating from the protein buffer), were observed to bind in the active site of *Tb*NDRT. The fragments bind with their ring systems essentially all binding to the same region of the pocket, in close proximity to the glycerol, which binds deep in the hydrophilic "tip" of the active site. By comparison with the X-ray structure of the ribosylated ester intermediate of *Lactobacillus helveticus* NDRT (with a ribose moiety bound covalently and adenine bound non-covalently), it could be seen that the aromatic fragments bind in a similar position to the adenine ring, whereas the glycerol mimics part of the bound ribose. The ligand binding sites observed shed new light on opportunities for the design of higher affinity inhibitors, and all four fragments showed some inhibition of *T. brucei brucei* growth *in vitro* (Table 1). Whether this effect was on target was not, however, investigated, and the fragments will require elaboration to improve affinity.

Targeting triosephosphate isomerase

In an early form of an X-ray crystallographic fragment screen against a putative NTD target, Verlinde et al. (1997) screened three cocktails of 128 fragments each against *T. brucei* triose-phosphate isomerase (*Tb*TIM). For one of the three cocktails, additional electron density was identified; however, the poor resolution (2.8 Å) prevented identification of the fragment, and subsequent soaks with subsets of the 128 fragments failed to reveal the ligand. This was possibly due to production of a binder from the chemical reaction of two ligands. Significant improvements to the method of X-ray crystallographic fragment screening along with several important technological advances has led to this approach now being used with great success both in the NTD drug discovery field as illustrated by examples discussed here, and in other areas (Murray and Blundell 2010).

Fragment-based Approaches in Antileishmanial Drug Discovery

Leishmaniases are a group of diseases caused by protozoan parasites of the genus *Leishmania* that are transmitted by *Phlebotomus* sandflies during a blood meal. It is estimated that there are between 700,000 to one million new cases each year, resulting in 20–30,000 deaths (WHO 2018e). There are three main forms of leishmaniasis:

(i) Visceral leishmaniasis—a disease characterized by bouts of fever, weight loss, anemia, and an enlarged spleen and liver. If untreated, it is fatal in > 95% of cases. There are estimated to be 50–90,000 new cases each year, predominantly in Brazil, East Africa and South-East Asia.

(ii) Cutaneous leishmaniasis—a disease characterized by skin lesions on exposed parts of the body that can cause permanent scarring. With an estimated 600,000–1 million new cases each year, it is the most common form of leishmaniasis, with most cases occurring in the Americas, the Mediterranean basin, the Middle East and Central Asia.

(iii) Mucocutaneous leishmaniasis—a disease in which the mucous membranes of the nose, mouth and throat are destroyed. The disease is predominantly found in Bolivia, Brazil, Ethiopia and Peru.

Currently, there is no vaccine to prevent leishmaniases, and disease prevention relies primarily on reducing contact with sandflies. Leishmaniases are currently treated with pentavalent antimonial compounds that have been in use for several decades, as well as the newer drugs amphotericin B, paramomycin and miltefosine. However, as yet, drugs are not available to those in need, and only miltefosine can be administered orally. Furthermore, as current therapies do not clear parasites from the body, treatment

failure, relapse and mortality are high among HIV co-infected patients unless antiretroviral therapy is given (WHO 2018e).

Although there is a need for new therapies, the development of antileishmanials is challenging as drugs must not only be able to traverse multiple membranes to gain access to the amastigote-stage parasite that resides within macrophages and other mononuclear phagocytic cells, but must also be stable to the acidic pH of macrophages. Fewer published examples of fragment-based approaches being applied primarily to the discovery of antileishmanials can be found, as compared with the number of published fragment-based approaches applied to antitrypanosomal drug discovery. Some examples are discussed below and summarized in Table 2.

Table 2. Examples of fragment-based approaches applied to antileishmanial drug discovery.

Target	Approach	Selected fragment hit(s)	Elaborated compound	Reference
L. major coproporphyrinogen III oxidase	X-ray crystallographic fragment screen	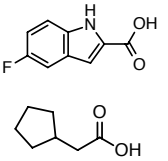	N/A	Verlinde et al. (2009)
L. major adenylate kinase	X-ray crystallographic fragment screen	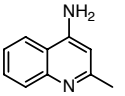	N/A	Verlinde et al. (2009)
L. naiffi uracil-DNA glycosylase	X-ray crystallographic fragment screen followed by enzyme assay	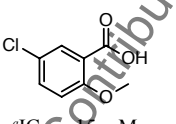 [a]IC_{50} = 15 mM [b]LE = 0.21 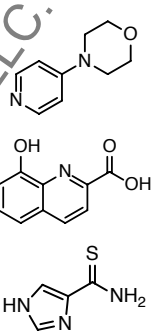	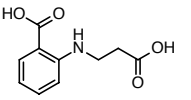 IC_{50} = 15 µM LE = 0.44	Verlinde et al. (2009)
L. amazonensis and *L. donovani*	Whole-cell screen of 1604 fragments	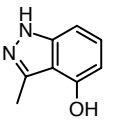 [c]EC_{50} = 4 µM 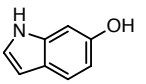 EC_{50} = 31 µM	N/A	Ayotte et al. (2018)

[a]IC_{50}, concentration causing 50% inhibition as measured in enzyme assays; [b]LE, ligand efficiency = (−RTln(IC_{50}))/NHA in kcal.mol^{-1}.NHA; [c]EC_{50}, half maximal effective concentration as measured in whole-cell assays.

Screening fragments by X-ray crystallography to identify novel chemical starting points for antileishmanial drug design

The MSGPP Consortium performed a number of X-ray crystallographic fragment screens to identify chemical starting points for inhibitors of leishmanial proteins crystallized by the consortium (Verlinde et al. 2009). A collection of fragment cocktails created in-house (the Biomolecular Structure Center (BMSC) collection), which was also used in the X-ray crystallographic fragment screens performed against *Tb*NDRT and *Tc*HisRS described in the previous section, was utilized for the screens.

Crystals of *L. major* coproporphyrinogen III oxidase, an enzyme involved in porphyrin biosynthesis, were soaked with 66 different fragment cocktails. Co-crystal structures were obtained for two fragments each from different cocktails (Table 2). Interestingly, one of the two fragment hits, cyclopentyl acetate, was observed to bind at three positions within the active site. In the same structure, one molecule of acetate (co-purified with the enzyme) was also bound. The four carboxylates contributed by the three fragment molecules and the acetate molecule were predicted to occupy the binding sites of the four carboxylates of the natural substrate coproporphyinogen-III.

Crystals of a putative *L. major* adenylate kinase were also soaked with fragment cocktails, and a single fragment hit—4-amino-2-methyl-quinoline—binding to the protein was identified (Table 2).

Uracil-DNA glycosylase (UDG) catalyses excision of misincorporated uracil from DNA and initiates "base-excision repair" (Pena-Diaz et al. 2004). Having solved the structure of a putative uracil-DNA glycosylase from *Leishmania naiffi*, crystals of the enzyme were soaked with 68 cocktails each containing ten fragments. Four fragments were observed to bind to the enzyme (Table 2), as was DMSO. A derivative of one fragment hit (5-chloro-2-methoxybenzoic acid) was designed and found to inhibit the activity of the enzyme 1000-fold more potently than the parent fragment (IC_{50} = 15 μM (LE = 0.44) vs 15 mM (LE = 0.21); Table 2). Recently, and since this fragment screen, Mishra et al. (2018) have shown that expression of the gene coding for UDG is upregulated in *Leishmania donovani* in response to treatment with commonly used antileishmanial drugs, and that drug-resistant clinical isolates of *L. donovani* show higher levels of the transcript encoding UDG. For these reasons, the enzyme has been proposed as a potential target for new combination therapies. The hits identified here may therefore serve as good starting points for development of tool compounds/new drugs targeting this enzyme.

Fragment-based phenotypic screening to identify leishmanicidal agents

Ayotte et al. (2018) used a hybrid strategy incorporating aspects of a fragment-based approach and a phenotypic screen, to identify fragments with leishmanicidal activity. From an initial set of 8000 fragments, a library of 1604 fragments was compiled. The starting set was refined using cheminformatic filters (to enrich for desirable substructures and maximize chemical diversity), as well as ^{1}H NMR analysis (to ensure all compounds included in the library were sufficiently soluble, and showed no signs of degradation or aggregation). The library was tested in 169 pools of 7–12 compounds against axenic cultures of promastigote-stage *Leishmania amazonensis* and *L. donovani* parasites, each at a concentration of 166 μM. Fifty fragment pools were found to show high leishmanicidal activity against both parasites at this concentration, as determined by microscopic examination, and 16 of these showed selectivity (having little/no cytotoxic effect on macrophages). Subsequently, fragments in the five pools showing the greatest leishmanicidal activity but no cytotoxic effect on macrophages, were tested individually at the same concentration. In this process, two fragments with selective leishmanicidal activity were identified (Table 2). These compounds—an indazole and an indole—were subsequently also shown to inhibit intracellular amastigote-stage *L. amazonesis* parasites within murine bone-marrow derived macrophages (EC_{50} values of 4 and 31 μM, determined respectively, Table 2), and have no effect on the macrophages even at a concentration of 500 μM (corresponding to a selectivity index > 125 for the most active compound). Interestingly, indoles and indazoles are scaffolds of a number of published leishmanicidal lead compounds. Close analogues of the two hits were also tested to establish structure-activity relationships, and in the process two compounds with modest increases

(2.8–3.7-fold) in potency were identified, as were modifications that were detrimental to the activity. The activity and selectivity of the lead indole and indazoles identified warrant further investigations into their potential as lead leishmanicidal compounds and/or tool compounds to reveal novel targets.

Fragment-based Approaches in Dengue Drug Discovery

Dengue is a viral infection that is transmitted by female *Aedes* mosquitoes, primarily of the species *Aedes aegypti*. The disease is widespread in tropical and subtropical regions, and has an increasing global incidence due to a growing number of outbreaks and spread to previously unaffected regions (WHO 2017). Although it is difficult to quantify the disease burden, it has been estimated that there are 390 million infections per year, and 96 million people presenting with clinical manifestations (Bhatt et al. 2013). The dengue virus (DENV) gives rise to flu-like symptoms, from which a patient typically recovers within 2–7 days (WHO 2018f). However, in a small proportion of patients, the disease develops into potentially lethal Dengue Haemorrhagic Fever (also known as severe dengue) or Dengue Shock Syndrome (Rajapakse 2011). Four DENV serotypes (DENV-1, DENV-2, DENV-3 and DENV-4) cause dengue in humans, and although infection with one serotype provides lifelong immunity to that serotype, it increases the risk of developing severe dengue upon subsequent infection with another serotype (WHO 2018f). Currently, there are no specific drugs for prevention or treatment of dengue, and disease control relies primarily on reducing contact with mosquitoes (WHO 2018a). Dengvaxia®, the first Dengue vaccine, was licensed in 2015 and approved for use in 9–45 year olds in endemic areas of 20 countries. However, retrospective analysis has revealed that the vaccine confers an increased risk of severe dengue to those not previously infected and as such is only recommended in persons with evidence of a previous infection (WHO 2018f). Currently, disease treatment is limited to supportive care and fluid resuscitation (WHO 2009), and as such small molecule drugs that could be used for chemoprophylaxis/treatment could be transformative.

The DENV has an approximately 11 kb, positive-sense, single-strand RNA genome, encoding three structural proteins and seven non-structural proteins (NS) (Noble et al. 2010). These virus-encoded proteins, along with host proteins required for viral replication, have been explored as potential antiviral drug targets (Behnam et al. 2016). The examples discussed below and summarized in Table 3, illustrate how fragment-based approaches have been used to target four DENV-encoded proteins.

Targeting DENV protease using principles of a fragment-based approach

The NS2B-NS3 protease complex is one of the best-studied targets for the development of drugs against the DENV (Behnam et al. 2016). This complex catalyzes the post-translational cleavage of the DENV polyprotein and is essential for viral replication; the proteolytic activity is localized to the N-terminus of NS3, while NS2B contributes to substrate recognition (Nitsche et al. 2014). A number of inhibitors of the DENV protease have been identified and these can be broadly classified into (i) peptidic and peptidomimetic inhibitors and (ii) non-peptidic small molecule inhibitors (reviewed by Nitsche et al. (2014)).

Behnam et al. (2014) utilized a fragment merging strategy to improve the potency of the tripeptide Bz-Arg-Lys-Nle-NH_2 found in a previous study (Nitsche et al. 2012) to inhibit DENV-2 protease (compound **24**, Figure 5, IC_{50} = 13.3 μM, K_i = 11.2 μM). Guided by docking studies performed using the DENV-3 protease crystal structure, they synthesized and tested a series of peptides with different C-terminal moieties. Replacement of the C-terminal residue with a phenylglycine moiety improved activity fourfold (peptide **25**, Figure 5, IC_{50} = 3.3 μM, K_i = 2.1 μM). Furthermore, they were able to improve the activity a further fivefold by merging the peptide with previously identified peptide **26** (Figure 5, IC_{50} = 2.5 μM, K_i = 1.8 μM) with a variant N-terminal cap associated with improved membrane permeability, protease inhibitor activity, and antiviral activity (Nitsche et al. 2013) (peptide **27**, Figure 5, IC_{50} = 0.6 μM, K_i = 0.4 μM).

In a follow up study, Behnam et al. (2015) applied a fragment growing strategy to improve activity against the DENV protease, as well as the related West Nile virus (WNV). Initially, a benzyloxyether was added at the *para* position of the C-terminal phenylglycine moiety of peptide **25** (peptide **28**, Figure 5), which improved potency against the DENV-2 protease ninefold (IC_{50} = 0.367 μM) and WNV protease by 80-fold

Table 3. Examples of fragment-based approaches applied to anti-DENV drug discovery.

Target	Approach	Selected fragment hit(s)	Elaborated compound	Reference
NS2B-NS3	Fragment merging and growing	N/A	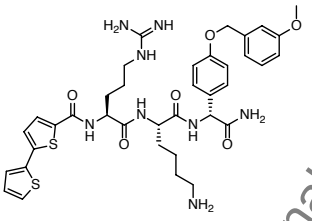 **32** [a]K_i (DENV-2 protease) = 176 nM [b]EC_{50} (DENV-2) = 3.4 μM	Figure 5 Behnam et al. (2014), Behnam et al. (2015)
RdRp	X-ray crystallographic screen of 1408 fragments. Elaboration by growing	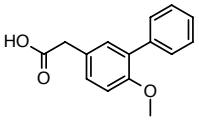 **35** [c]IC_{50} (DENV-4 RdRp) = 730 μM [d]K_D (DENV-3 & 4 RdRp) = 210 and 610 μM [e]LE = 0.24–0.28	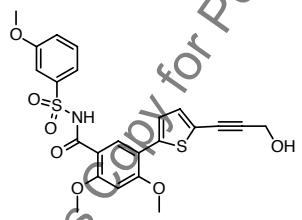 **40** IC_{50} (DENV-4 RdRp) = 0.17 μM K_D (DENV-4 RdRp) = 0.07 μM LE = 0.30 EC_{50} (DENV-1-4) = 1.8–2.3 μM	Figure 6 Noble et al. (2016), Yokokawa et al. (2016)
MTase	DSF screen of 500 fragments, followed by X-ray crystallography and enzyme assays. Elaboration by fragment linking	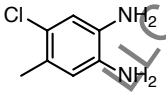 **41** [f]IC_{50} (2'*O*) = 9.3 mM LE = 0.28 [g]IC_{50} (N7) ≥ 10 mM 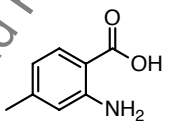 **42** IC_{50} (2'*O*) = 2.8 mM LE = 0.32 IC_{50} (N7) ≥ 10 mM	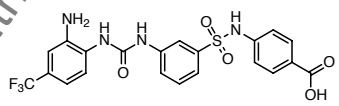 **45** IC_{50} (2'*O*) = 91 μM LE = 0.16 IC_{50} (N7) = 1.1 mM 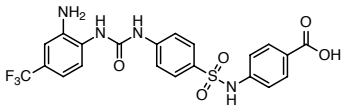 **46** IC_{50} (2'*O*) = 110 μM LE = 0.16 IC_{50} (N7) = 742 μM 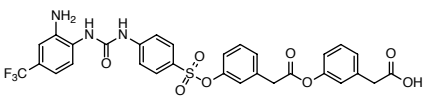 **47** IC_{50} (2'*O*) = 24 μM LE = 0.15	Coutard et al. (2014), Benmansour et al. (2017), Hernandez et al. (2019)

[a]K_i, inhibition constant; [b]EC_{50}, half maximal effective concentration as measured in whole-cell assays; [c]IC_{50}, concentration causing 50% inhibition as measured in enzyme assays; [d]K_D, dissociation constant; [e]LE, ligand efficiency = (−RTln(K_D/IC_{50}))/NHA, in kcal.mol^{-1}.NHA^{-1}; [f]IC_{50} (2'*O*), IC_{50} determined in a 2'-*O*-MTase assay using DENV-3 MTase; [g]IC_{50} (N7), IC_{50} determined in a N7-MTase assay using DENV-3 MTase.

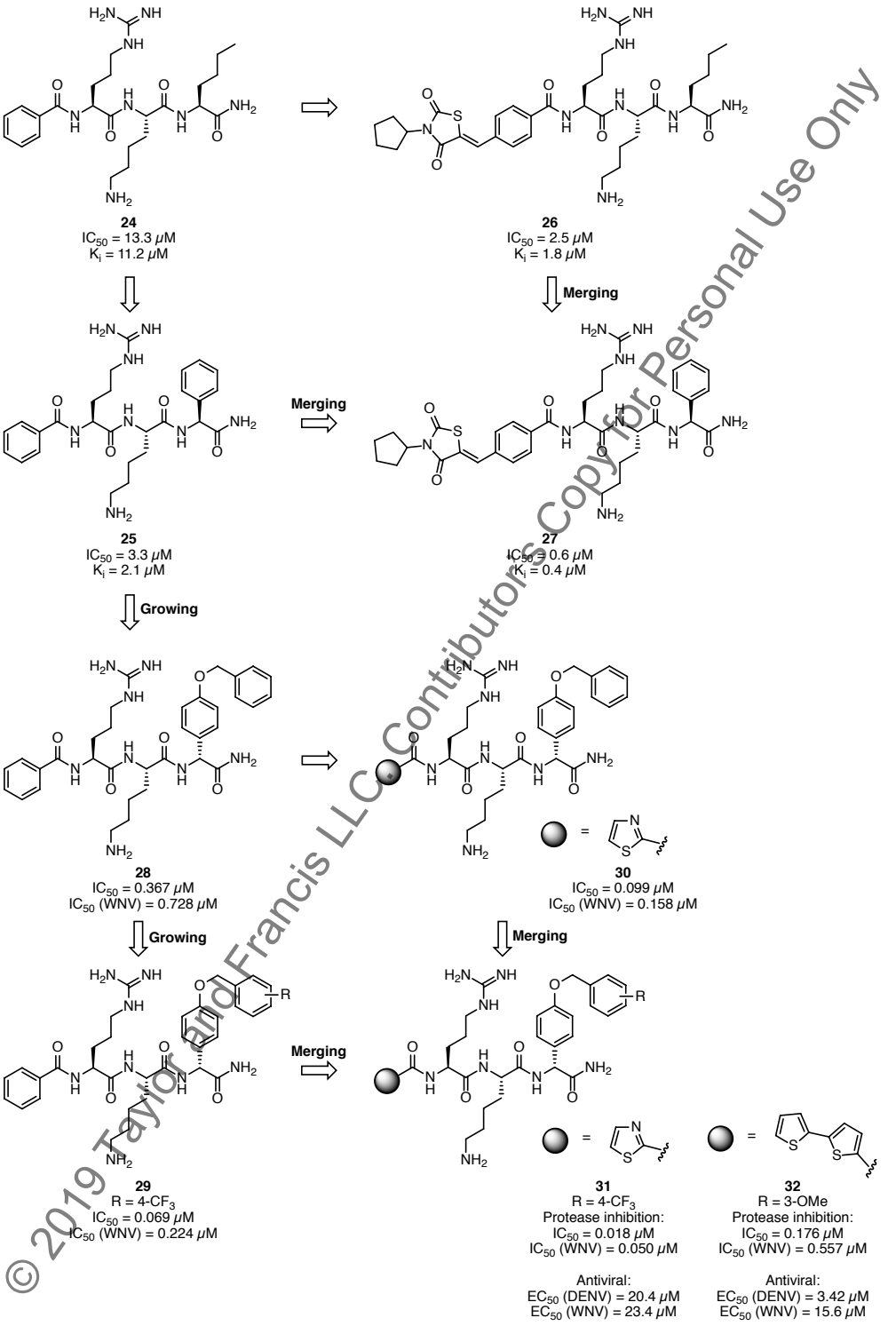

Figure 5. Fragment merging and growing strategies applied to the optimization of a peptidic inhibitor of DENV-2 protease. Unless otherwise specified, IC_{50} and K_i values shown were determined from DENV-2 protease activity assays. As indicated, IC_{50} values for inhibition of the WNV protease and for antiviral activity against DENV-2 and WNV are also shown in some cases.

(IC_{50} = 0.728 μM). Subsequent addition of a trifluoromethyl group (peptide **29**, Figure 5) led to a further fivefold improvement in activity against the DENV-2 protease (IC_{50} = 0.069 μM) and threefold improvement against the WNV protease (IC_{50} = 0.224 μM). In parallel, they searched for the optimal N-terminal cap; a range of peptide **28** derivatives in which the benzoyl moiety was replaced with various small chemical groups was tested. Substitution of the benzoyl moiety with a thiazole ring (peptide **30**) produced the most potent inhibitor of DENV-2 and WNV protease (IC_{50} = 0.099 and 0.158 μM, respectively). The most productive N and C terminal modifications were then combined into a single molecule through merging of peptides **29** and **30**. The resultant peptide (**31**) was observed to inhibit DENV-2 and WNV protease with IC_{50} values of 18 and 50 nM, respectively, corresponding to a 180-fold increase in activity against the DENV-2 protease and a > 1000-fold increase in activity against WNV protease relative to peptide **25**. Furthermore, peptide **31** also possesses antiviral activity against both DENV-2 and WNV (EC_{50} = 20.4 and 23.4 μM, respectively). However, a less potent inhibitor of DENV-2 protease showed the highest antiviral activity (peptide **32**, Figure 5, EC_{50}(DENV) = 3.42 μM and EC_{50}(WNV) = 15.6 μM), presumably due to improved permeability.

Targeting RNA polymerase

DENV RNA-dependent RNA polymerase (RdRp) forms the C-terminal part of NS5, the largest DENV protein and the most highly conserved protein across the DENV serotypes (Yap et al. 2007). The N-terminus of NS5 functions as a methyltransferase (discussed in the next section). DENV RdRp is an attractive drug target because it is required for viral replication, has no mammalian counterpart, and because its conservation across DENV serotypes should facilitate identification of inhibitors effective against all serotypes (Lim et al. 2015). Furthermore, viral polymerases have been clinically-validated as drug targets (Tsai et al. 2006), and X-ray crystal structures of DENV RdRp have been determined (Yap et al. 2007, Zhao et al. 2015), enabling structure-based drug design. Nucleoside and non-nucleoside inhibitors of RdRp have been identified to date, with some nucleoside inhibitors having entered clinic trials, albeit with limited success (reviewed by Lim et al. 2015, Behnam et al. 2016).

Researchers at Novartis previously performed a HTS campaign against RdRp (Yin et al. 2009, Niyomrattanakit et al. 2010). *N*-Sulfonyl anthranilic acid **33** (Figure 6a), which inhibits DENV-2 RdRp with an IC_{50} value of 7.2 μM, was identified as a hit in this screen. Subsequent SAR investigations and optimization led to a highly lipophilic molecule (compound **34**, Figure 6a) with improved activity against the enzyme (IC_{50} = 0.26 μM), but without antiviral activity in cell cultures (Yin et al. 2009). As the HTS campaign failed to produce specific DENV RdRp inhibitors with suitable physicochemical properties, a fragment-based approach was explored as an alternative method to identify lead compounds targeting RdRp.

Noble et al. (2016) screened the Novartis library of 1408 fragments in pools of eight against RdRp using X-ray crystallography. DENV-3 RdRp crystals were soaked with a total of 176 fragment pools, with each fragment tested at a concentration of 625 μM. This led to the identification of a single fragment hit (compound **35**) that was subsequently shown by SPR to bind DENV-3 and DENV-4 RdRp with K_D values of 210 and 610 μM, respectively (LE = 0.28 and 0.24, respectively). The structure of DENV-3 RdRp, like that of other polymerases, resembles a right hand with subdomains that mimic the fingers, palm and thumb. The fragment hit was observed to bind in a novel allosteric pocket of *apo* DENV-3 RdRp, between the thumb and palm subdomains and the priming loop that regulates binding of the RNA template and polymerization. Importantly, binding at this site was also shown to translate into an inhibitory effect on enzyme activity, with an IC_{50} value of 730 μM determined against DENV-4 RdRp in a *de novo* initiation/elongation assay. Replacement of the terminal phenyl moiety of fragment **35** with a thiophene produced a fragment (**36**, Figure 6b) with two-to-seven-fold improved affinity and the same binding mode. Guided by X-ray crystallography, this thiophene fragment was subsequently elaborated using a fragment growing strategy (Yokokawa et al. 2016).

As shown in Figure 6b, initially a propargyl alcohol moiety was added to fill a narrow cavity in the protein and displace a water molecule. This modification increased the affinity by > 100-fold. The subsequent removal of a methylene group and addition of a methyl group improved affinity by a further

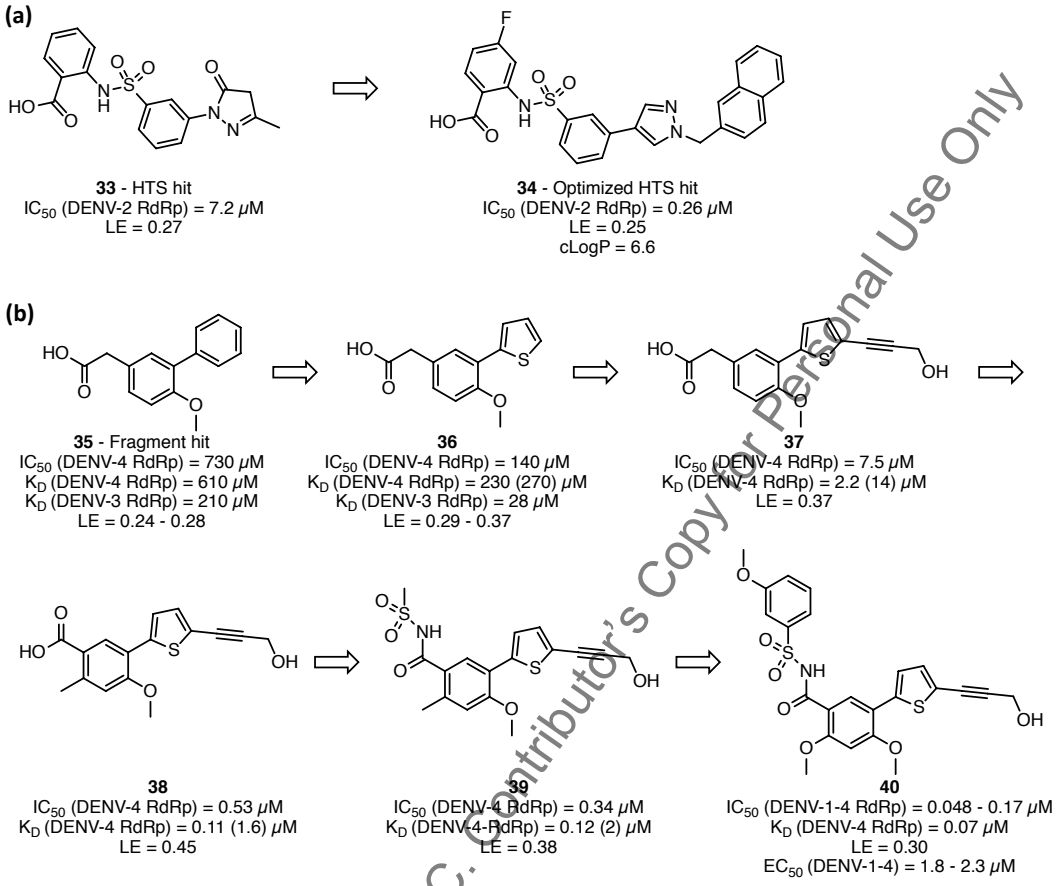

Figure 6. HTS and fragment-based approaches targeting DENV RdRp. (a) HTS hit and *N*-sulfonyl anthranilic acid lead. **(b)** Fragment hit and the growing strategy by which the compound was elaborated into a more potent DENV RdRp inhibitor. K_D values determined by SPR are shown, with the corresponding K_D values obtained by isothermal titration calorimetry shown in brackets where determined.

1.3 and 15-fold, respectively (**38**, Figure 6b). Yokokawa et al. (2016) next sought to replace the carboxylic acid moiety in the original fragment hit with a bioisostere. Acylsulfonamide **39** showed comparable binding affinity to compound **38**, but lacked anti-DENV activity at concentrations up to 50 µM, possibly due to poor cellular permeability. A co-crystal structure of compound **39** confirmed that the binding mode of the parent fragment was retained, and that the propargyl alcohol and acylsulfonamide moieties formed two and three hydrogen-bonds with the protein, respectively. They additionally showed that the methyl group of the acylsulfonamide was solvent exposed. With the aim of improving the physicochemical properties without reducing affinity for the enzyme, various replacements for this methyl group were investigated. Ultimately, replacement of the methyl substituent with a 3-methoxyphenyl substituent produced compound **40**, which binds RdRp with a K_D of 0.07 µM (DENV-4) and inhibits DENV-1-4 RdRp with IC_{50} values of 0.05–0.17 µM (Figure 6b), corresponding to a > 4000-fold improvement in activity relative to the parent fragment, and a slight overall improvement in ligand efficiency (0.30). Importantly, this compound demonstrated anti-DENV activity against all four DENV serotypes, with EC_{50} values between 1.8 and 2.3 µM measured, and the antiviral activity was demonstrated to be on target (Lim et al. 2016). The study by Yokokawa et al. (2016) is the first to describe RdRp inhibitors with pan-serotype antiviral activity in cell cultures.

Targeting DENV helicase and methyltransferase

Coutard et al. (2014) utilized a fragment-based approach to target two key components of the DENV replication complex, the NS3 Helicase (Hel) and the NS5 methyltransferase (MTase). Hel forms the C-terminus of the NS3 protein, and catalyzes activities involved in RNA capping and replication of the DENV genome—nucleotide and RNA triphosphate hydrolysis and RNA unwinding (Benarroch et al. 2004, Yon et al. 2005). MTase forms the N-terminus of the NS5 protein, and catalyzes two sequential methylation reactions involved in formation of the cap structure at the 5'-end of the RNA genome: (i) methylation of the cap guanine at the N7-position, and (ii) methylation at the 2'-*O*-position of the first nucleotide that is transcribed (Dong et al. 2010). The Hel and N7-MTase activities are essential for viral replication, and while moderate replication is possible when 2'-*O*-MTase activity is defective, 2'-*O*-MTase activity is required for virulence *in vivo* (Matusan et al. 2001, Dong et al. 2010, Zust et al. 2013). These findings highlight the potential of Hel and MTase as novel targets for antiviral therapies for the prevention or treatment of dengue. As crystal forms of DENV NS3 Hel and NS5 MTase yielding high-resolution X-ray structures had previously been obtained (Luo et al. 2008, Lim et al. 2011), Coutard et al. (2014) anticipated that the proteins would be suitable for targeting using a fragment-based approach.

In an attempt to identify novel binding sites and/or starting points for inhibitor development, a library of 500 rule-of-three compliant fragments was screened against each of the target proteins using DSF. In this primary screen, in which fragments were tested at a concentration of 2 mM, 36 and 32 fragments increased the melting temperature of Hel (from DENV-4) and MTase (from DENV-3) by > 0.5ºC, respectively, consistent with binding. These fragments were therefore progressed to X-ray crystallography experiments for hit confirmation and binding mode determination. Unfortunately, in the case of Hel, crystal-soaking experiments did not produce a single fragment co-crystal structure and as such none of the fragment hits were confirmed by X-ray crystallography. By contrast, a total of seven fragments were observed by X-ray crystallography to bind *S*-adenosyl-L-methionine (SAM)-bound DENV-3 MTase. Furthermore, the seven fragments were found to bind at four distinct sites—one fragment was observed to bind in a site overlapping with the GTP binding site, while the remaining six fragments bind at one of three novel binding sites. The inhibitory effect of the MTase fragment hits on DENV-3 MTase activity was also determined and five of the seven X-ray crystallography-confirmed hits were found to inhibit 2'-*O*-MTase activity with IC_{50} values between 180 μM and 9 mM, with the most active 2'-*O*-MTase inhibitor also inhibiting N7-MTase activity (IC_{50} = 2 mM). Notably, the fragment binding at the GTP-binding site showed little-to-no inhibition of MTase activity. Hel and MTase inhibitors were also found among Hel and MTase fragment hits that did not yield crystal structures in soaking experiments (or, where attempted, co-crystallization experiments); however, because detailed knowledge of a fragment's binding mode is important for fragment elaboration, these fragments were not progressed. The failure to obtain any Hel-fragment co-crystal structures despite some of the DSF fragment hits possessing weak inhibitory activity against the enzyme in an ATPase assay, was hypothesized to be a consequence of the fragment hits inducing a conformational change in the protein that cannot occur in the crystal; previous studies had shown the protein to be highly dynamic (Luo et al. 2008).

In a subsequent study, two of the MTase fragment hits (fragments **41** and **42**, Table 3, Figure 7) were used as the basis for a fragment-linking strategy aimed at developing higher affinity and selective DENV MTase inhibitors (Benmansour et al. 2017). The two fragments selected were observed to bind in adjacent positions in a novel binding site in close proximity to the binding site of the natural substrate SAM (Figure 7). Informed by docking experiments, different linking strategies were considered. Compounds in which the fragments were linked by a 3-unit urea or amide linker were predicted to allow the fragments to adopt their desired binding poses and form linker-mediated hydrogen bonding interactions, and were therefore synthesized. A few close analogues were also synthesized, the design of which was inspired by a third fragment hit observed to bind in a site overlapping with fragment **41**. Crystal soaking experiments yielded co-crystal structures for two urea-linked compounds, demonstrating that they are able to bind MTase; however, the binding site of the two analogues is shifted relative to the parent fragments (e.g.,

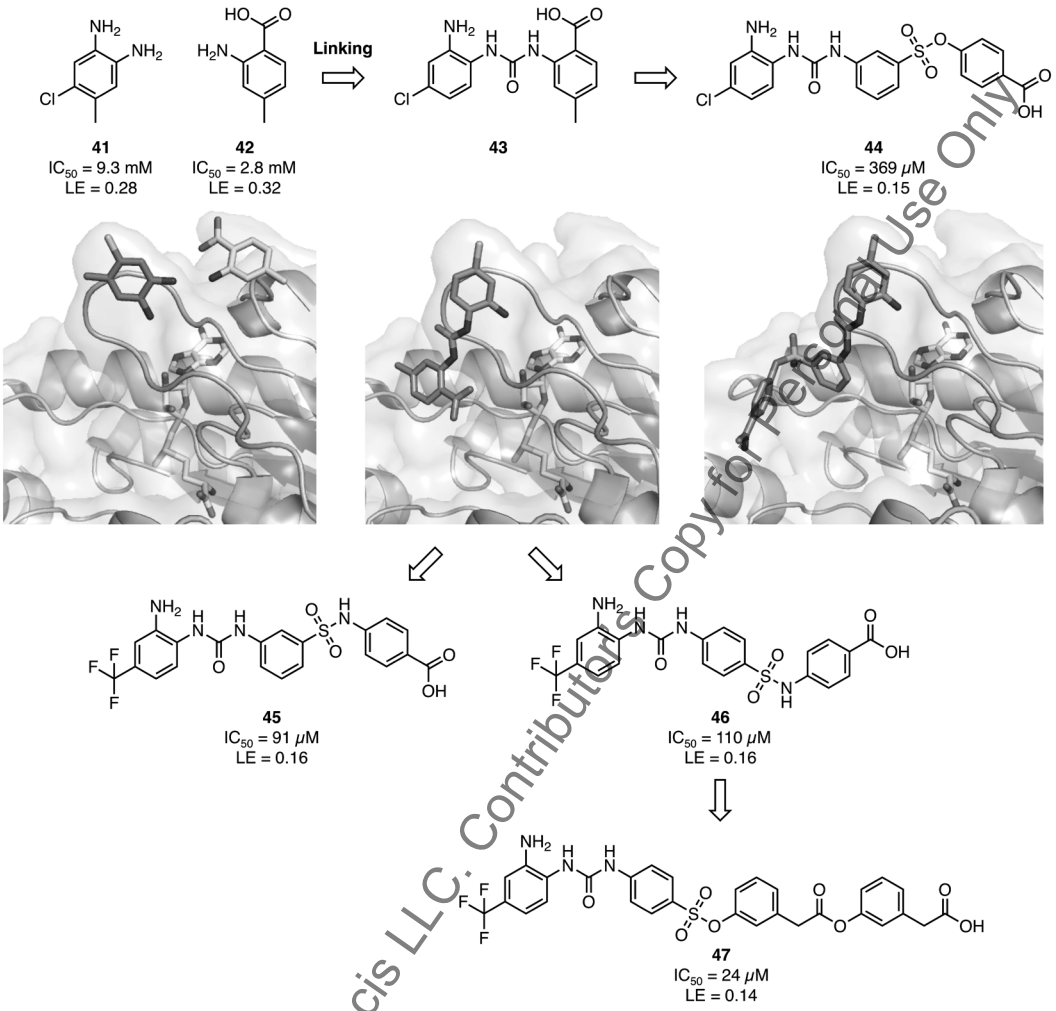

Figure 7. Fragment-based approach to targeting DENV MTase. Crystal structures showing binding of fragment hits **41** and **42** (carbons in magenta or cyan, respectively) and elaborated compounds **43** and **44** (carbons in orange) to DENV-3 MTase (with bound SAM, carbons in yellow) [PDB IDs: 5EKX, 5EIF, 5EC8 and 5EHG]. IC_{50} values measured in a 2'-*O*-MTase activity assay, and the corresponding LE values in kcal.mol^{-1}.NHA, are shown.

Color version at the end of the book

compound **43**, Figure 7). Sulfonamide and sulfone ester derivatives of the new urea-linked compounds designed to pick up additional interactions in adjacent areas of the MTase binding site were synthesized, soaked into DENV-3 MTase crystals and tested for inhibition of DENV-3 MTase activity. Co-crystal structures were obtained for two of the derivatives and showed that the binding mode of the original urea-linked compounds was maintained (e.g., compound **44**, Figure 7). The most active compounds (compounds **45** and **46**, Figure 7), which did not give rise to co-crystal structures, inhibit 2'-*O*-MTase activity with IC_{50} values of 91 and 110 μM. Although this represents a 25–100-fold improvement in the IC_{50} values relative to the parent fragments, this corresponds to a substantial drop in ligand efficiency relative to the parent fragments (Table 3, Figure 7). However, favorably, by contrast with the parent fragments, the elaborated compounds also inhibit N7-MTase activity (IC_{50} values of 1.1 and 0.7 mM for compound **45** and **46**, respectively). Unfortunately, however, when tested for antiviral activity against strains of DENV-1–3 in Vero E6 cells, no antiviral activity was detected at concentrations up to 20 μM. An elaborated sulfone ester analogue of **46** with approximately four-fold improved inhibitory activity in a DENV 2'-*O*-MTase

assay was subsequently identified (**47**, Figure 7) (Hernandez et al. 2019). However, the analogue, which was without cytotoxicity at concentrations ≤ 100 μM, was also without effect on DENV-2 replication *in vitro* at concentrations ≤ 20 μM. Nevertheless, these studies have now produced a number of fragment and inhibitor co-crystal structures that could inform the future development of compounds with improved MTase inhibitory activity that also possess antiviral activity and have improved selectivity compared to known inhibitors, which primarily bind in the SAM binding site (Behnam et al. 2016).

Conclusions

Drug discovery in a NTD landscape is associated with a number of challenges. New drugs should be cheap and ideally orally administered to ensure they are accessible to those in need. Furthermore, NTDs are complex and diverse, and low investment, disproportionate to the disease burden, means there are fewer validated targets and often a lack of *in vivo* relevant assays compatible with HTS platforms (Martin-Plaza and Chatelain 2015). However, with new public-private partnerships entering the area, this is changing. Phenotypic screening is the favored hit finding mechanism in NTD drug discovery and has produced clinical candidates, e.g., fexinidazole and the oxaborole SCYX-7158 for the treatment of HAT (Hotez et al. 2016). Nonetheless, phenotypic screening is not without its shortcomings. For example, the approach requires access to screening libraries difficult to handle and maintain outside of an industry setting, and libraries invariably represent limited chemical space. Furthermore, it can be challenging to optimize HTS hits while achieving appropriate physicochemical properties. In this regard, fragment-based approaches, although target-based, have the key advantages that libraries are smaller and more efficiently explore chemical space, and more careful control of physicochemical properties is possible during optimization. Fragments are also valuable tools for identifying novel allosteric sites in a target (which can facilitate selective targeting), as seen in the fragment-based approaches targeting *Tc*SpdSyn and DENV RdRP, as well as binding hotspots. For these reasons, fragment-based approaches certainly hold value in NTD drug discovery either alone (provided they are paired with careful target validation) or in conjunction with phenotypic screening approaches.

In addition to the requirement for a well-validated target, a successful fragment-based approach generally also demands a target that can be expressed in a pure and soluble form and is suitable for binding mode studies by X-ray crystallography/protein NMR, as iterative structure determination is important for informing fragment elaboration. Fragment screens make use of a range of predominantly biophysical techniques from DSF, which is fast and inexpensive and employs a RT-PCR machine likely present in most academic institutions, to more specialized approaches like NMR and X-ray crystallography. As illustrated by the DENV Hel example discussed, the ability to obtain structural information on fragment binding remains a bottleneck. A number of the fragment-based approaches discussed involved an X-ray crystallography-based primary or secondary fragment screen, which is advantageous in that the binding mode is known early on. This, however, requires access to specialist equipment and expertise. Notably, the MSGPP Consortium has made significant contributions to the field, both in the form of structures and fragment cocktails for X-ray crystallography-based fragment screens. *In silico* approaches are also widely used, both in fragment screening and to guide fragment elaboration. However, it is important to be aware that experimental binding modes can deviate from those predicted, and *in silico* approaches will invariably identify only fragments binding to pre-formed pockets. Variations on a classical fragment-based approach are also being employed, for example, whole-cell screening of fragments, two examples of which were presented, and although innovation is welcomed, whether such approaches can produce optimizable hits remains to be seen.

The challenge, as with other target-based approaches, remains translating potency against an isolated target to on-target activity in cell cultures under *in vivo*-relevant conditions. Many of the published fragment-based approaches discussed here report only on fragment hit identification and as yet have not reached this hurdle, and at least in one case—the study targeting *Tb*PTR1—translation of potent enzyme inhibition to whole-cell activity proved difficult. Nonetheless, several other examples of fragment-based approaches producing on-target cell-active compounds—and in the case of compounds targeting *Tb*PEX14-PEX5, also with activity in an animal model—are presented, and we eagerly watch this space.

References

Amano, Y., I. Namatame, Y. Tateishi, K. Honboh, E. Tanabe, T. Niimi et al. 2015. Structural insights into the novel inhibition mechanism of *Trypanosoma cruzi* spermidine synthase. Acta Crystallogr. D Biol. Crystallogr. 71: 1879–1889.

Ayotte, Y., F. Bilodeau, A. Descoteaux and S.R. LaPlante. 2018. Fragment-based phenotypic lead discovery: cell-based assay to target leishmaniasis. ChemMedChem. 13: 1377–1386.

Bauer, S., K. Kemter, A. Bacher, R. Huber, M. Fischer and S. Steinbacher. 2003. Crystal structure of *Schizosaccharomyces pombe* riboflavin kinase reveals a novel ATP and riboflavin-binding fold. J. Mol. Biol. 326: 1463–1473.

Behnam, M.A., C. Nitsche, S.M. Vechi and C.D. Klein. 2014. C-Terminal residue optimization and fragment merging: discovery of a potent peptide-hybrid inhibitor of dengue protease. ACS Med. Chem. Lett. 5: 1037–1042.

Behnam, M.A., D. Graf, R. Bartenschlager, D.P. Zlotos and C.D. Klein. 2015. Discovery of nanomolar dengue and West Nile virus protease inhibitors containing a 4-benzyloxyphenylglycine residue. J. Med. Chem. 58: 9354–9370.

Behnam, M.A., C. Nitsche, V. Boldescu and C.D. Klein. 2016. The medicinal chemistry of dengue virus. J. Med. Chem. 59: 5622–5649.

Benarroch, D., B. Selisko, G.A. Locatelli, G. Maga, J.L. Romette and B. Canard. 2004. The RNA helicase, nucleotide 5'-triphosphatase, and RNA 5'-triphosphatase activities of Dengue virus protein NS3 are Mg^{2+}-dependent and require a functional Walker B motif in the helicase catalytic core. Virology. 328: 208–218.

Benmansour, F., I. Trist, B. Coutard, E. Decroly, G. Querat, A. Brancale et al. 2017. Discovery of novel dengue virus NS5 methyltransferase non-nucleoside inhibitors by fragment-based drug design. Eur. J. Med. Chem. 125: 865–880.

Bhatt, S., P.W. Gething, O.J. Brady, J.P. Messina, A.W. Farlow, C.L. Moyes et al. 2013. The global distribution and burden of dengue. Nature. 496: 504–507.

Birkholtz, L.M., M. Williams, J. Niemand, A.I. Louw, L. Persson and O. Heby. 2011. Polyamine homoeostasis as a drug target in pathogenic protozoa: peculiarities and possibilities. Biochem. J. 438: 229–244.

Blaazer, A.R., K.M. Orrling, A. Shanmugham, C. Jansen, L. Maes, E. Edink et al. 2015. Fragment-based screening in tandem with phenotypic screening provides novel antiparasitic hits. J. Biomol. Screen. 20: 131–140.

Bosch, J., M.A. Robien, C. Mehlin, E. Boni, A. Riechers, F.S. Buckner et al. 2006. Using fragment cocktail crystallography to assist inhibitor design of *Trypanosoma brucei* nucleoside 2-deoxyribosyltransferase. J. Med. Chem. 49: 5939–5946.

Coutard, B., E. Decroly, C. Li, A. Sharff, J. Lescar, G. Bricogne et al. 2014. Assessment of Dengue virus helicase and methyltransferase as targets for fragment-based drug discovery. Antiviral. Res. 106: 61–70.

Dardonville, C., E. Rinaldi, M.P. Barrett, R. Brun, I.H. Gilbert and S. Hanau. 2004. Selective inhibition of *Trypanosoma brucei* 6-phosphogluconate dehydrogenase by high-energy intermediate and transition-state analogues. J. Med. Chem. 47: 3427–3437.

Dawidowski, M., L. Emmanouilidis, V.C. Kalel, K. Tripsianes, K. Schorpp, K. Hadian et al. 2017. Inhibitors of PEX14 disrupt protein import into glycosomes and kill Trypanosoma parasites. Science. 355: 1416–1420.

de Koning, H.P., M.K. Gould, G.J. Sterk, H. Tenor, S. Kunz, E. Luginbuehl et al. 2012. Pharmacological validation of *Trypanosoma brucei* phosphodiesterases as novel drug targets. J. Infect. Dis. 206: 229–237.

Dong, H., D.C. Chang, X. Xie, Y.X. Toh, K.Y. Chung, G. Zou et al. 2010. Biochemical and genetic characterization of dengue virus methyltransferase. Virology. 405: 568–578.

Durrant, J.D., L. Hall, R.V. Swift, M. Landon, A. Schnaufer and R.E. Amaro. 2010. Novel naphthalene-based inhibitors of *Trypanosoma brucei* RNA editing ligase 1. PLoS Negl. Trop. Dis. 4: e803.

Durrant, J.D., A.J. Friedman and J.A. McCammon. 2011. CrystalDock: a novel approach to fragment-based drug design. J. Chem. Inf. Model. 51: 2573–2580.

Erlanson, D.A., S.W. Fesik, R.E. Hubbard, W. Jahnke and H. Jhoti. 2016. Twenty years on: the impact of fragments on drug discovery. Nat. Rev. Drug Discov. 15: 605–619.

Erlanson, D.A. 2019. April 16. Third fragment-based drug approved! [Blog post]. http://practicalfragments.blogspot.com/2019/04/third-fragment-based-drug-approved.html.

Ettari, R., L. Tamborini, I.C. Angelo, N. Micale, A. Pinto, C. De Micheli et al. 2013. Inhibition of rhodesain as a novel therapeutic modality for human African trypanosomiasis. J. Med. Chem. 56: 5637–5658.

Fairlamb, A.H., P. Blackburn, P. Ulrich, B.T. Chait and A. Cerami. 1985. Trypanothione: a novel bis(glutathionyl) spermidine cofactor for glutathione reductase in trypanosomatids. Science. 227: 1485–1487.

Gilbert, I.H. 2013. Drug discovery for neglected diseases: molecular target-based and phenotypic approaches. J. Med. Chem. 56: 7719–7726.

Haanstra, J.R., E.B. Gonzalez-Marcano, M. Gualdron-Lopez and P.A. Michels. 2016. Biogenesis, maintenance and dynamics of glycosomes in trypanosomatid parasites. Biochim. Biophys. Acta. 1863: 1038–1048.

Hanau, S., E. Rinaldi, F. Dallocchio, I.H. Gilbert, C. Dardonville, M.J. Adams et al. 2004. 6-Phosphogluconate dehydrogenase: a target for drugs in African trypanosomes. Curr. Med. Chem. 11: 2639–2650.

Hann, M.M., A.R. Leach and G. Harper. 2001. Molecular complexity and its impact on the probability of finding leads for drug discovery. J. Chem. Inf. Comput. Sci. 41: 856–864.

Hernandez, J., L. Hoffer, B. Coutard, G. Querat, P. Roche, X. Morelli et al. 2019. Optimization of a fragment linking hit toward Dengue and Zika virus NS5 methyltransferases inhibitors. Eur. J. Med. Chem. 161: 323–338.

Hopkins, A.L., C.R. Groom and A. Alex. 2004. Ligand efficiency: a useful metric for lead selection. Drug Discov. Today. 9: 430–431.

Hotez, P.J., B. Pecoul, S. Rijal, C. Boehme, S. Aksoy, M. Malecela et al. 2016. Eliminating the neglected tropical diseases: translational science and new technologies. PLoS Negl. Trop. Dis. 10: e0003895.

Kalidas, S., I. Cestari, S. Monnerat, Q. Li, S. Regmi, N. Hasle et al. 2014. Genetic validation of aminoacyl-tRNA synthetases as drug targets in *Trypanosoma brucei*. Eukaryot. Cell. 13: 504–516.

Karthikeyan, S., Q. Zhou, A.L. Osterman and H. Zhang. 2003. Ligand binding-induced conformational changes in riboflavin kinase: structural basis for the ordered mechanism. Biochemistry. 42: 12532–12538.

Koh, C.Y., A.B. Wetzel, W.J. de van der Schueren and W.G. Hol. 2014. Comparison of histidine recognition in human and trypanosomatid histidyl-tRNA synthetases. Biochimie. 106: 111–120.

Koh, C.Y., L.K. Siddaramaiah, R.M. Ranade, J. Nguyen, T. Jian, Z. Zhang et al. 2015. A binding hotspot in *Trypanosoma cruzi* histidyl-tRNA synthetase revealed by fragment-based crystallographic cocktail screens. Acta Crystallogr. D Biol. Crystallogr. 71: 1684–1698.

Krauth-Siegel, R.L. and M.A. Comini. 2008. Redox control in trypanosomatids, parasitic protozoa with trypanothione-based thiol metabolism. Biochim. Biophys. Acta. 1780: 1236–1248.

Lim, S.P., L.S. Sonntag, C. Noble, S.H. Nilar, R.H. Ng, G. Zou et al. 2011. Small molecule inhibitors that selectively block dengue virus methyltransferase. J. Biol. Chem. 286: 6233–6240.

Lim, S.P., C.G. Noble and P.Y. Shi. 2015. The dengue virus NS5 protein as a target for drug discovery. Antiviral. Res. 119: 57–67.

Lim, S.P., C.G. Noble, C.C. Seh, T.S. Soh, A. El Sahili, G.K. Chan et al. 2016. Potent allosteric dengue virus NS5 polymerase inhibitors: mechanism of action and resistance profiling. PLoS Pathog. 12: e1005737.

Luo, D., T. Xu, R.P. Watson, D. Scherer-Becker, A. Sampath, W. Jahnke et al. 2008. Insights into RNA unwinding and ATP hydrolysis by the flavivirus NS3 protein. EMBO J. 27: 3209–3219.

Martin-Plaza, J. and E. Chatelain. 2015. Novel therapeutic approaches for neglected infectious diseases. J. Biomol. Screen. 20: 3–5.

Matusan, A.E., M.J. Pryor, A.D. Davidson and P.J. Wright. 2001. Mutagenesis of the dengue virus type 2 NS3 protein within and outside helicase motifs: effects on enzyme activity and virus replication. J. Virol. 75: 9633–9643.

McKerrow, J.H., P.S. Doyle, J.C. Engel, L.M. Podust, S.A. Robertson, R. Ferreira et al. 2009. Two approaches to discovering and developing new drugs for Chagas disease. Mem. Inst. Oswaldo Cruz. 104 Suppl. 1: 263–269.

McShan, D., S. Kathman, B. Lowe, Z. Xu, J. Zhan, A. Statsyuk et al. 2015. Identification of non-peptidic cysteine reactive fragments as inhibitors of cysteine protease rhodesain. Bioorg. Med. Chem. Lett. 25: 4509–4512.

Merritt, E.A., T.L. Arakaki, J.R. Gillespie, E.T. Larson, A. Kelley, N. Mueller et al. 2010. Crystal structures of trypanosomal histidyl-tRNA synthetase illuminate differences between eukaryotic and prokaryotic homologs. J. Mol. Biol. 397: 481–494.

Mishra, A., M.I. Khan, P.K. Jha, A. Kumar, S. Das, P. Das et al. 2018. Oxidative stress-mediated overexpression of uracil DNA glycosylase in *Leishmania donovani* confers tolerance against antileishmanial drugs. Oxid. Med. Cell Longev. 2018: 4074357.

Mpamhanga, C.P., D. Spinks, L.B. Tulloch, E.J. Shanks, D.A. Robinson, I.T. Collie et al. 2009. One scaffold, three binding modes: novel and selective pteridine reductase 1 inhibitors derived from fragment hits discovered by virtual screening. J. Med. Chem. 52: 4454–4465.

Murray, C.W. and T.L. Blundell. 2010. Structural biology in fragment-based drug design. Curr. Opin. Struct. Biol. 20: 497–507.

Nitsche, C., M.A. Behnam, C. Steuer and C.D. Klein. 2012. Retro peptide-hybrids as selective inhibitors of the Dengue virus NS2B-NS3 protease. Antiviral. Res. 94: 72–79.

Nitsche, C., V.N. Schreier, M.A. Behnam, A. Kumar, R. Bartenschlager and C.D. Klein. 2013. Thiazolidinone-peptide hybrids as dengue virus protease inhibitors with antiviral activity in cell culture. J. Med. Chem. 56: 8389–8403.

Nitsche, C., S. Holloway, T. Schirmeister and C.D. Klein. 2014. Biochemistry and medicinal chemistry of the dengue virus protease. Chem. Rev. 114: 11348–11381.

Niyomrattanakit, P., Y.L. Chen, H. Dong, Z. Yin, M. Qing, J.F. Glickman et al. 2010. Inhibition of dengue virus polymerase by blocking of the RNA tunnel. J. Virol. 84: 5678–5686.

Noble, C.G., Y.L. Chen, H. Dong, F. Gu, S.P. Lim, W. Schul et al. 2010. Strategies for development of Dengue virus inhibitors. Antiviral. Res. 85: 450–462.

Noble, C.G., S.P. Lim, R. Arora, F. Yokokawa, S. Nilar, C.C. Seh et al. 2016. A conserved pocket in the dengue virus polymerase identified through fragment-based screening. J. Biol. Chem. 291: 8541–8548.

Oberholzer, M., G. Marti, M. Baresic, S. Kunz, A. Hemphill and T. Seebeck. 2007. The *Trypanosoma brucei* cAMP phosphodiesterases TbrPDEB1 and TbrPDEB2: flagellar enzymes that are essential for parasite virulence. FASEB J. 21: 720–731.

Orrling, K.M., C. Jansen, X.L. Vu, V. Balmer, P. Bregy, A. Shanmugham et al. 2012. Catechol pyrazolinones as trypanocidals: fragment-based design, synthesis, and pharmacological evaluation of nanomolar inhibitors of trypanosomal phosphodiesterase B1. J. Med. Chem. 55: 8745–8756.

Pedrique, B., N. Strub-Wourgaft, C. Some, P. Olliaro, P. Trouiller, N. Ford et al. 2013. The drug and vaccine landscape for neglected diseases (2000–11): a systematic assessment. Lancet Glob. Health. 1: e371–379.

Pena-Diaz, J., M. Akbari, O. Sundheim, M.E. Farez-Vidal, S. Andersen, R. Sneve et al. 2004. *Trypanosoma cruzi* contains a single detectable uracil-DNA glycosylase and repairs uracil exclusively via short patch base excision repair. J. Mol. Biol. 342: 787–799.

Peplow, M. 2017. Astex shapes CDK4/6 inhibitor for approval. Nat. Biotechnol. 35: 395–396.

Pham, J.S., K.L. Dawson, K.E. Jackson, E.E. Lim, C.F. Pasaje, K.E. Turner et al. 2014. Aminoacyl-tRNA synthetases as drug targets in eukaryotic parasites. Int. J. Parasitol. Drugs Drug Resist. 4: 1–13.

Rajapakse, S. 2011. Dengue shock. J. Emerg. Trauma Shock. 4: 120–127.

Ruda, G.F., G. Campbell, V.P. Alibu, M.P., Barrett, R. Brenk and I.H. Gilbert. 2010. Virtual fragment screening for novel inhibitors of 6-phosphogluconate dehydrogenase. Bioorg. Med. Chem. 18: 5056–5062.

Ruddigkeit, L., R. van Deursen, L.C. Blum and J.L. Reymond. 2012. Enumeration of 166 billion organic small molecules in the chemical universe database GDB-17. J. Chem. Inf. Model. 52: 2864–2875.

Schmunis, G.A. and Z.E. Yadon. 2010. Chagas disease: a Latin American health problem becoming a world health problem. Acta Trop. 115: 14–21.

Scott, D.E., A.G. Coyne, S.A. Hudson and C. Abell. 2012. Fragment-based approaches in drug discovery and chemical biology. Biochemistry. 51: 4990–5003.

Shibata, S., Z. Zhang, K.V. Korotkov, J. Delarosa, A. Nayuni, A.M. Kelley et al. 2011. Screening a fragment cocktail library using ultrafiltration. Anal. Bioanal. Chem. 401: 1585–1591.

Sienkiewicz, N., H.B. Ong and A.H. Fairlamb. 2010. *Trypanosoma brucei* pteridine reductase 1 is essential for survival *in vitro* and for virulence in mice. Mol. Microbiol. 77: 658–671.

Spinks, D., H.B. Ong, C.P. Mpamhanga, E.J. Shanks, D.A. Robinson, I.T. Collie et al. 2011. Design, synthesis and biological evaluation of novel inhibitors of *Trypanosoma brucei* pteridine reductase 1. ChemMedChem. 6: 302–308.

Steverding, D., D.W. Sexton, X. Wang, S.S. Gehrke, G.K. Wagner and C.R. Caffrey. 2012. *Trypanosoma brucei:* chemical evidence that cathepsin L is essential for survival and a relevant drug target. Int. J. Parasitol. 42: 481–488.

Tsai, C.H., P.Y. Lee, V. Stollar and M.L. Li. 2006. Antiviral therapy targeting viral polymerase. Curr. Pharm. Des. 12: 1339–1355.

Verlinde, C.L., H. Kim, B.E. Bernstein, S.C. Mande and W.G. Hol. 1997. Anti-trypanosomiasis drug development based on structures of glycolytic enzymes. pp. 365–394. *In*: P. Veerapandian [ed.]. Structure-based Drug Design. Marcel Dekker Inc, New York.

Verlinde, C.L., E. Fan, S. Shibata, Z. Zhang, Z. Sun, W. Deng et al. 2009. Fragment-based cocktail crystallography by the Medical Structural Genomics of Pathogenic Protozoa Consortium. Curr. Top. Med. Chem. 9: 1678–1687.

Vincent, I.M. and M.P. Barrett. 2015. Metabolomic-based strategies for anti-parasite drug discovery. J. Biomol. Screen. 20: 44–55.

WHO. 2009. Dengue: guidelines for diagnosis, treatment, prevention and control—New edition. World Health Organization.

WHO. 2017. Integrating neglected tropical diseases into global health and development: fourth WHO report on neglected tropical diseases. World Health Organization.

WHO. 2018a. Neglected tropical diseases. World Health Organization. https://www.who.int/neglected_diseases/diseases/en/ (accessed December 12, 2018).

WHO. 2018b. Chagas disease (American Trypanosomiasis)—Epidemiology. World Health Organization. https://www.who.int/chagas/epidemiology/en/ (accessed December 12, 2018).

WHO. 2018c. Trypanosomiasis, human African (sleeping sickness). World Health Organization. https://www.who.int/news-room/fact-sheets/detail/trypanosomiasis-human-african-(sleeping-sickness) (accessed December 12, 2018).

WHO. 2018d. WHO outlines criteria to assess elimination of sleeping sickness. World Health Organization. https://www.who.int/neglected_diseases/news/criteria-eliminate-sleeping-sickness/en/ (accessed December 12, 2018).

WHO. 2018e. Leishmaniasis. World Health Organization. https://www.who.int/leishmaniasis/en/ (accessed December 12, 2018).

WHO. 2018f. Dengue and severe dengue. World Health Organization. https://www.who.int/news-room/fact-sheets/detail/dengue-and-severe-dengue (accessed December 12, 2018).

Yap, T.L., T. Xu, Y.L. Chen, H. Malet, M.P. Egloff, B. Canard et al. 2007. Crystal structure of the dengue virus RNA-dependent RNA polymerase catalytic domain at 1.85-angstrom resolution. J. Virol. 81: 4753–4765.

Yin, Z., Y.L. Chen, R.R. Kondreddi, W.L. Chan, G. Wang, R.H. Ng et al. 2009. *N*-Sulfonylanthranilic acid derivatives as allosteric inhibitors of dengue viral RNA-dependent RNA polymerase. J. Med. Chem. 52: 7934–7937.

Yokokawa, F., S. Nilar, C.G. Noble, S.P. Lim, R. Rao, S. Tania et al. 2016. Discovery of potent non-nucleoside inhibitors of dengue viral RNA-dependent RNA polymerase from a fragment hit using structure-based drug design. J. Med. Chem. 59: 3935–3952.

Yon, C., T. Teramoto, N. Mueller, J. Phelan, V.K. Ganesh, K.H. Murthy et al. 2005. Modulation of the nucleoside triphosphatase/RNA helicase and 5'-RNA triphosphatase activities of Dengue virus type 2 nonstructural protein 3 (NS3) by interaction with NS5, the RNA-dependent RNA polymerase. J. Biol. Chem. 280: 27412–27419.

Zhao, Y., T.S. Soh, J. Zheng, K.W. Chan, W.W. Phoo, C.C. Lee et al. 2015. A crystal structure of the Dengue virus NS5 protein reveals a novel inter-domain interface essential for protein flexibility and virus replication. PLoS Pathog. 11: e1004682.

Zust, R., H. Dong, X.F. Li, D.C. Chang, B. Zhang, T. Balakrishnan et al. 2013. Rational design of a live attenuated dengue vaccine: 2'-*O*-methyltransferase mutants are highly attenuated and immunogenic in mice and macaques. PLoS Pathog. 9: e1003521.